

## **PHYSICS LABORATORY**

**VIVEK SAGAR PRASHANSA GUPTA AND ATUL SINGH ARORA**



**Advanced Optics Lab**

**Dr. Mandip Singh**  
**Indian Institute of Science Education and Research, Mohali**

**January-April, 2013**

Vivek Sagar Prashansa Gupta and Atul Singh Arora: *Physics Laboratory*, Advanced Optics Lab,

*I have no special talent. I am only passionately curious.*  
*Einstein*

## ACKNOWLEDGEMENTS

---

I express my sincere gratitude to our instructor Dr. Mandip Singh for his guidance and for providing an enjoyable laboratory experience. His insightful questions and discussions helped us extract the physics out of the experiments.

I also thank Vivek Sagar (MS11017) and Prashansa Gupta (MS11021) for their valuable contribution to this report as my team members, who made the task of performing experiments immensely comfortable and productive at the same time.



## CONTENTS

---

<b>1</b>	<b>MICHELSON INTERFEROMETER</b>	<b>1</b>
1.1	Aim	1
1.2	Theory	1
1.2.1	Determining Wavelength	2
1.2.2	Resolving the D-Lines	3
1.2.3	Subtle Points	4
1.2.4	'Practical' Theory	5
1.3	Procedure	5
1.3.1	Obtaining the ring	5
1.3.2	Finding $\lambda_{\text{average}}$	6
1.3.3	Finding $\lambda_{\text{separation}}$	6
1.4	Observations and Conclusion	7
1.5	Sources of error	7
<b>2</b>	<b>ACOUSTIC DIFFRACTION</b>	<b>11</b>
2.1	Theory	11
2.2	Further Questions	12
2.3	Calculations and Results	12
<b>3</b>	<b>NMR</b>	<b>17</b>
3.1	$T_1, T_2$	17
3.1.1	Minimal Introductory Theory	17
3.1.2	Instrumentation Setup	21
3.1.3	Theory	23
3.1.4	Practical Implementation	28
3.1.5	Observations	29
3.2	Diffusion	31
3.2.1	Theory	31
3.2.2	Practical Implementation	34
3.2.3	Observations and Result	35
<b>4</b>	<b>ZEEMAN EFFECT</b>	<b>37</b>
4.1	Introduction	37
4.2	Classical Description of Zeeman Splitting	37
4.2.1	Modeling the Atom as a harmonic oscillator	37
4.2.2	Zeeman Splitting and Polarization	38
4.2.3	Limitations	39
4.3	Fabry Parot	40
4.3.1	The effect of sources and lenses	40
4.4	Constant Deviation Spectrometer	42
4.5	The Setup	42
4.5.1	The 'TV' Zeeman (polarization)	42
4.5.2	The 'Prism' Zeeman (splitting)	43
<b>5</b>	<b>FABRY PEROT</b>	<b>49</b>
5.1	Calibrating the Fabry Perot	49

5.2	Determining the Space Between the Mirrors of the Etalon	49
5.2.1	Small Angle Approximation	51
5.3	The setup	51
5.4	Observations and Results	51

## LIST OF FIGURES

---

Figure 1	Equivalent Michelson Interferometer Setup	2
Figure 2	Observations for $\lambda_{\text{average}}$	8
Figure 3	Observations for $\lambda_{\text{difference}}$	9
Figure 4	Setup for Acoustic Diffraction	13
Figure 5	Graph	14
Figure 6	Observations	15
Figure 7	Calculations and Results	16
Figure 8	$T_1$ , peak 1	31
Figure 9	$T_1$ , peak 2	32
Figure 10	$T_2$ , peak 1	33
Figure 11	$T_2$ , peak 2	34
Figure 12	$\log(\text{Intensity})$ vs Gradient Percentage <sup>2</sup>	36
Figure 13	Split Distance vs Current	45
Figure 14	Calibration of Magnetic Field and Current	46
Figure 15	'Prism' Zeeman Setup	47
Figure 16	'TV' Zeeman Setup	48
Figure 17	The Fabry Perot Setup	53

## LIST OF TABLES

---

gfx/T1	29
gfx/T2	30
gfx/diffusion	36
gfx/zeemanReading	43
gfx/zeemanCalibration	44
gfx/fabryPerotDistance	51
gfx/fabryPerotDistanceResult	52
gfx/fabryPerotCalibration	52

gfx/fabryPerotCalibrationResult 52

## ACRONYMS

---

## MICHELSON INTERFEROMETER

---

August 8 and 19, 2013

### 1.1 AIM

To determine

1. the average wavelength of a monochromatic source
2. the difference in wavelengths of a dichromatic source (Sodium Light)

and to obtain White Light fringes.

### 1.2 THEORY

The Michelson interferometer demonstrates interference by *division of amplitude* of a wave by partial reflection. The apparatus consists of a source of light, two highly polished plane mirrors, a detector, a beam splitter and a compensating plate. The beam splitter is highly polished at the rear face in order to minimise reflections from the front face. The compensating plate made of the same material and adjusted parallel to beam splitter, essentially makes the path distance travelled in glass by both the beams equal, since one ray undergoes internal reflection while the other undergoes an external reflection; this is important in case the light is not monochromatic (for e.g white light) since refractive index changes with wavelength.

When light from the source falls on the beam splitter, it is partially reflected and partially transmitted in orthogonal directions. These two beams reach the mirrors and are then reflected back into the detector. The fringes can be seen by looking into the mirror through the beam splitter.

[Figure 1](#)<sup>1</sup> explains the formation of fringes. It can be understood by considering replacement of the real mirror  $M_2$  by its virtual image  $M'_2$  formed by reflection in  $G_1$ .  $M'_2$  is parallel to  $M_1$ . We may now think of the source as forming two virtual images  $L_1$  and  $L_2$  in  $M_1$  and  $M'_2$ . Looking at the mirror  $M_1$ , one can see  $M_1$  along with the virtual image  $M'_2$  of  $M_2$  formed in  $G_1$ . The air film enclosed between  $M_1$  and  $M'_2$  is wedge shaped, and we obtain straight line

---

<sup>1</sup> Taken from Jenkins White

fringes. Circular fringes are obtained when the interferometer is in normal adjustment. Depending on the shape of this air film i.e the angle between the mirrors the fringes can be straight, circular, parabolic, elliptical, hyperbolic in shape.

In the given apparatus, both the mirrors can be moved with the help of screws and the distance moved can be measured with a precision of  $10^{-7}$  m. One of the mirrors is mounted on a carriage, whose movement mechanism consists of a large drum. One rotation of this drum moves the mirror by a millimetre. One part of a slow motion smaller drum moves the mirror by  $10^{-4}$  mm. The beam splitter and compensating plate are aligned at  $45^\circ$  to the interferometer arm. The mirrors are provided with two screws at the back which help tilt them so as to adjust them mutually perpendicular.

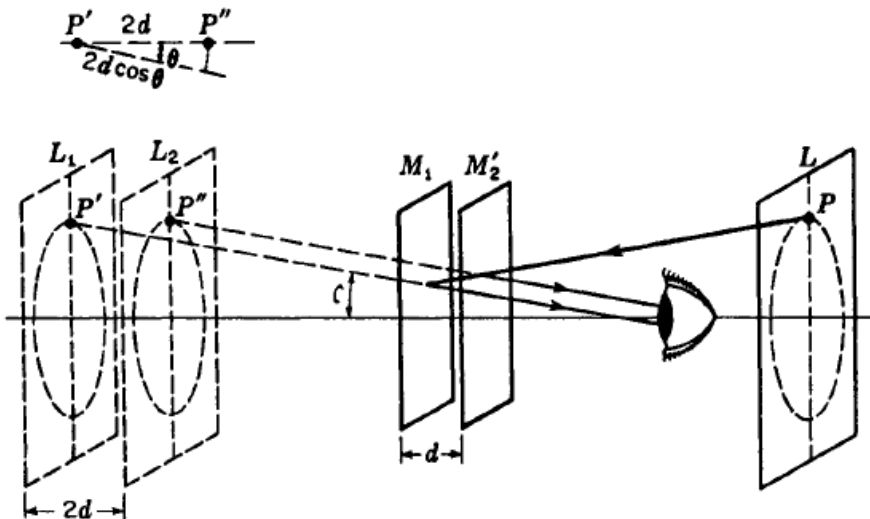


Figure 1: Equivalent Michelson Interferometer Setup

### 1.2.1 Determining Wavelength

The easiest place to begin the analysis of this apparatus would be to ignore the thickness of the beam splitter and the compensator (which is anyway not needed for this experiment) and assume the observations are made at the centre of a far away screen (although in the experiment we've used a lens to focus at infinity). Now at this point, the path difference in the two beams of light would be essentially because of twice the distance between the fixed mirror and the image of the movable mirror. Let this be given by  $2d$ , where  $d$  is the distance between the said mirrors. Now imagine a point other than the centre at the screen. The angle this makes with the principal axis, let

that be  $\theta$ . The distance light will travel for this point, which can cause phase difference will be  $2d \cos \theta$ . Keeping in mind the fact that there's an abrupt phase change of  $\pi$  because of reflection at the beam splitter, we have for destructive interference

$$2d \cos \theta = m\lambda \quad (1)$$

and similarly, for constructive interference we'll have

$$2d \cos \theta = (m + 1/2)\lambda \quad (2)$$

It is easy to put in a few numbers <sup>2</sup> and conclude that reducing the distance causes fringes to collapse to the centre (while the spacing between fringes increases).

Now experimentally, say for a given configuration, the centre's dark;

$$2d = m\lambda \quad (3)$$

where  $2d$  again, represents the distance between the mirrors, but that is not known experimentally. What is known experimentally is the position of the moveable mirror, with respect to some reference,  $d_i$ . Now we move this mirror to a new position, say  $d_f$ , such that  $N$  fringes have collapsed to the centre in the process. Then we have

$$2(d + (d_f - d_i)) = (m - N)/\lambda \quad (4)$$

Subtracting these, gives us a simple method of finding the 'average' wavelength of the sodium source

$$\lambda = 2(d_f - d_i)/N = 2\Delta D/N \quad (5)$$

### 1.2.2 Resolving the D-Lines

That was the basic theory behind the experiment. Using a little more naive Math, we can even find the small difference in the Sodium D-lines. Here's how we go about it. As a thought experiment, imagine that 'd' is made 0. Then the mirror is moved away (or towards) through a distance  $d$ . In general, the fringe patterns will overlap in some fashion. Assume a  $d$  is such that,

$$2d \cos \theta = m\lambda_1 \quad 2d \cos \theta = (m + 1/2)\lambda_2 \quad (6)$$

For small  $\theta$ , we can easily obtain

$$2d/\lambda_1 - 2d/\lambda_2 = 1/2 \quad (7)$$

Observe here what has happened. The maxima of one pattern falls on the minima of the other and vice versa. This means that what

---

<sup>2</sup> refer to page 15.23 of Ajoy Ghatak, Optics, 4th Edition for details

we obtain is all bright! Consequently, the pattern disappears in this situation. Making this general, if

$$2d/\lambda_1 - 2d/\lambda_2 = 1/2, 3/2, 5/2.. \quad (8)$$

then the fringe pattern will disappear and for 1, 2, 3 .. it will reappear. Now let us think about how this could be achieved in practice, as it is hard to find the precise location where  $d$  becomes zero. To get around this, we find the distance between occurrence of two blank (all bright) patterns. Assuming the unknown (to the experimenter) distance between the mirrors is  $d$ , but the position of the moveable mirror with respect to some reference, is again given by  $d_i$ . We can then write in general for some odd  $m$

$$2d(1/\lambda_1 - 1/\lambda_2) = m/2 \quad (9)$$

Now the moveable mirror is moved to a position  $d_f$  such that the same pattern is obtained. For this we then have

$$2(d + (d_f - d_i))(1/\lambda_1 - 1/\lambda_2) = m/2 - 1 \quad (10)$$

On subtracting, to eliminate the unknown  $d$ , we get

$$2\Delta d(\Delta\lambda/\lambda^2) = 1 \quad (11)$$

where  $\Delta d = d_f - d_i$ . So finally we have,

$$\Delta\lambda = \lambda^2 / 2\Delta d \quad (12)$$

and that's that.

### 1.2.3 Subtle Points

The theory discussed above is roughly sufficient. Finer points have been posed as questions

1. How does the diffuser help? Can the interference pattern be obtained without the diffuser?
2. What is the wavefront of the waves after they go through a diffuser?
3. Why are the fringes circular? Explain using Huygen's principle (the ray optic method is rather simple).
4. Are the fringes real or virtual?
5. If the light source was in fact a point source, what type of an interference pattern will you obtain? (courtesy sir)
6. In a typical YDSE setup, if we don't use a screen, are we expected to observe fringes?

7. How can we span all angles using just two knobs in the mirror?
8. Can you apply the idea of beats to explain the increase decrease of contrast?
9. What is the expected pattern for a plain wavefront?
10. For a plain wavefront, when a 'dark' pattern is obtained (you'll know once you solve the previous question), where does the energy of the electromagnetic wave disappear? (sir asked this)

#### 1.2.4 '*Practical*' Theory

Some more questions whose answers become clear after playing with the apparatus for sufficiently long

1. What is the primary source of the backlash error in the fine rotation knob?
2. When the average distance of the mirrors from the partly reflecting mirror is higher, why is it harder to get circular fringes?
3. What can cause a uniform rotation of the knob to screw (threaded cylinder) to not cause a corresponding change in the fringe pattern? (basically identify the main cause of this error)

### 1.3 PROCEDURE

#### 1.3.1 *Obtaining the ring*

It is assumed that you've setup the michelson interferometer in accordance with the diagram in Jenkins White.

1. Move the coarsely moveable mirror to (roughly) the smallest distance from the beam splitter.
2. Now move the other mirror to a slightly larger (you can use smaller also, but then the steps would change correspondingly) distance from the beam splitter, than that of the coarsely moveable mirror.
3. Ensure that the pin hole disk is being used.
4. Align the mirror using the three screws provided such that all the four spots coincide (you can choose to look directly without the telescope; in fact that works better usually).
5. Now remove the pin hole disk from the view and put the diffruser (if not already present).

6. Move the moveable mirror at most four times using the coarse movement drum (ensure the movement knob is unlocked) until the fringe pattern is observed. If the pattern is too dense (more than roughly 15 fringes), then follow from the mirror alignment step.
7. Assuming you have roughly 10 fringes at this stage, you now need to bring the centre of the rings into view (if it is already, you're running on beginner's luck).
  - a) There are two screws on the mirror and they can roughly be thought of as adjusting the X and Y offset.
  - b) You'll know you're on the right track if the fringes magnify as you adjust
  - c) Note that you must leave the knob to know where it really is. Simply holding it also causes the position of the knob to change.
8. If you want further magnification, you can continue rotating and aligning the centre as you go if the need be.

CAVEAT: For certain path differences, the contrast will become very low (as is clear from theory); don't panic.

### 1.3.2 *Finding $\lambda_{average}$*

Assuming you have obtained the ring already;

1. Set the movement to fine using the lock knob on the apparatus.
2. Place the telescope if you haven't done that already, such that one of the rings is just at the cross-wire.
3. Move the fine rotation knob until the fringes just start to move.
4. Now keep track of the rotations and count 20 fringes as they cross the cross-wire.
5. Repeat this to get sufficient observations

### 1.3.3 *Finding $\lambda_{separation}$*

Assuming you've obtained the ring;

1. Lock the movement to fine using the lock knob
2. Move the fine rotation until all the fringes disappear and just begin to appear
3. Note the position at this point

4. Now continue rotating the knob until the fringes disappear again and just begin to appear
5. Note this position again
6. Repeat this to get sufficient observations

#### 1.4 OBSERVATIONS AND CONCLUSION

In accordance with [Figure 2](#), the wavelength of sodium light (average) was found to be  $620 \pm 65\text{nm}$ . [Figure 3](#), the difference in wavelengths was found to be  $0.67 \pm 0.15\text{nm}$ .

#### 1.5 SOURCES OF ERROR

- The back and forth movement of the mirrors is not precise i.e. the mirrors do not remain parallel to the preceding positions. So the setup might not be normally adjusted and the fringes might not be circular.
- The large drum has a gear arrangement that is aligned to move with the thread of the screw. This calls for a significant amount of backlash error which means that while the screw moves, the fringes don't contribute to erroneous results.
- While noting the positions when the fringes reappear, the contrast of the fringes is noted by the human eye. This contrast almost does not vary over almost a rotation of the small screw.

S.No.	Initial reading	Final reading	d = Total width of 20 fringes *10^-7 m
1	42	107	65
2	23	96	73
3	65	117	52
4	20	76	56
5	76	148	72
6	52	120	68
7	20	83	63
8	83	151	68
9	55	108	53
10	8	64	56
11	64	119	55
12	19	90	71
13	30	100	70
14	10	69	59
15	73	130	57
16	60	114	54
17	30	84	54
18	84	139	55
19	94	160	66
20	10	72	62
21	95	158	63
22	58	120	62
23	0	71	71
24	5	65	60
25	58	124	66

Mean

62.04

Std. dev

6.569505309

Average wavelength of Na light = 620 nm

Abs. error = 65 nm

Figure 2: Michelson Interferometer: Observations

D = Distance between the fringes of minimum contrast * $10^{-7}$ m	
	2910
	2822
	2835
	2886
	2800
Mean	2850.6
Std dev	40.99560952

Separation between the fringes = 0.67 nm

Rel. error = 2(rel. error in  $\lambda$ ) + rel. error in D = 0.232

Abs error = 0.156 nm

Figure 3: Michelson Interferometer: Observations



# 2

## ACOUSTIC DIFFRACTION

---

August 26 and 27, 2013

### 2.1 THEORY

Certain assumptions made in the following discussion have been explicitly stated here for clarity.

1. The diffraction grating formed has almost zero thickness
2. A diffraction pattern is observed only when a standing wave is produced
3. Snell's law can be ignored in the consideration of the diffraction pattern

The idea of the experiment is to estimate the speed of sound in distilled water, by producing an acoustic diffraction grating. The setup is as shown in [Figure 4](#).

Debye and Sears, in 1932 demonstrated that light diffracts while it passes through a liquid medium excited to ultrasonic vibrations. They explained it by saying that the density maxima and minima of the standing wave obtained in the liquid behaved like an optical diffraction grating, where the grating constant was the wavelength of this ultrasonic wave. Therefore, this method can be used to determine the speed of sound in the medium once we have determined the wavelength of sound by measuring the distance between the ultrasonic source and the diffraction image.

The generation of standing wave in a medium causes changes in density due to pressure nodes and anti-nodes of the sound wave. These density fluctuations in turn cause variations in refractive index which diffracts a beam of light travelling perpendicular to the direction of sound as if it had been diffracted from a diffraction grating of spacing  $2d = \lambda_{\text{sound}}$  for a standing wave. The sound field is set up by driving a piezoelectric crystal at a given frequency.

The setup consists of a laser, an ultrasonic probe i.e. a piezoelectric crystal, a cuvette filled with a medium (in this case, distilled water), a screen and a frequency generator. The known result  $d \sin \theta = n\lambda$  is used for finding  $d$  and therefore  $\lambda_{\text{sound}}$ , where small angle approximation is used to write

$$\sin \theta = \frac{\text{in the plane of the screen, displacement from the centre}}{\text{distance of the grating from the screen}}$$

**BRAGG'S DIFFRACTION** An electromagnetic radiation which reflects from the surface of a substance has travelled less distance than the one which reflects from a plane of atoms inside the crystal. The penetrating electromagnetic radiation travels down to the internal layer, reflects, and travels back over the same distance before being back at the surface. The distance travelled depends on the separation of the layers and the angle at which the electromagnetic radiation entered the material. For this wave to be in phase with the wave which reflected from the surface it needs to have travelled a whole number of wavelengths while inside the material. Bragg expressed this in an equation now known as Bragg's Law, mathematically stated as

$$n\lambda = 2d \sin \theta$$

where  $\lambda$  is the wavelength of the incident radiation,  $d$  is the spacing between the scattering planes and  $\theta$  the angle between them. It gives the angles at which the radiation, reflected off the scattering plane interferes constructively and produces a peak (a Bragg peak). First proposed by William Lawrence Bragg and William Henry Bragg in 1912, it is used as a tool to study crystals in the form of X-ray and neutron diffraction.

## 2.2 FURTHER QUESTIONS

- Study braggs diffraction and raman diffraction from Photonics by Teichi
- How does the dimension of the medium affect the pattern?
- Can we realize Braggs diffraction in this experiment?
- Will the diffraction pattern change upon movement of the diffraction grating? Diffraction pattern formation in case no standing waves are formed?
- If the diffraction grating is infinite , will its movement affect the diffraction pattern — it will be phase shifted

## 2.3 CALCULATIONS AND RESULTS

The observations have been listed in [Figure 6](#). The results have been listed in [Figure 7](#). [Figure 5](#) is the graph obtained.

The speed of sound was found out to be 1312 m/s and 1250 m/s using either sides of the graph.

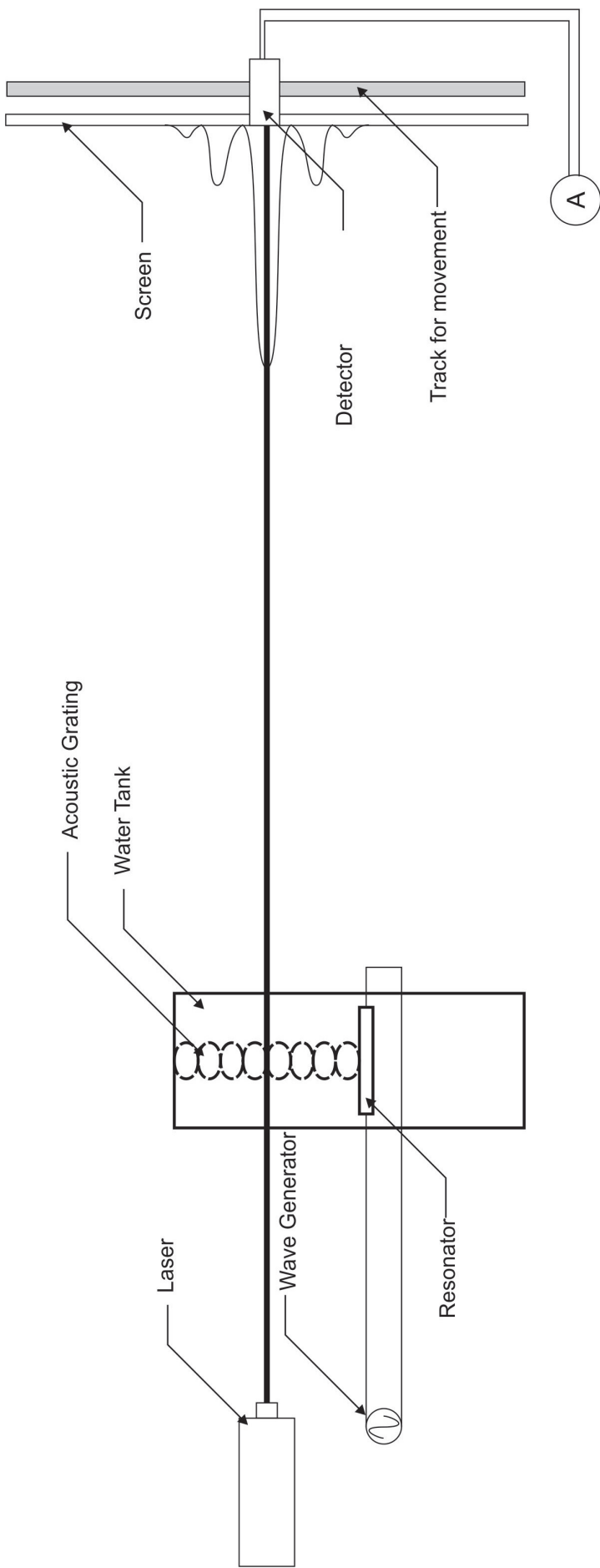


Figure 4: Setup for Acoustic Diffraction

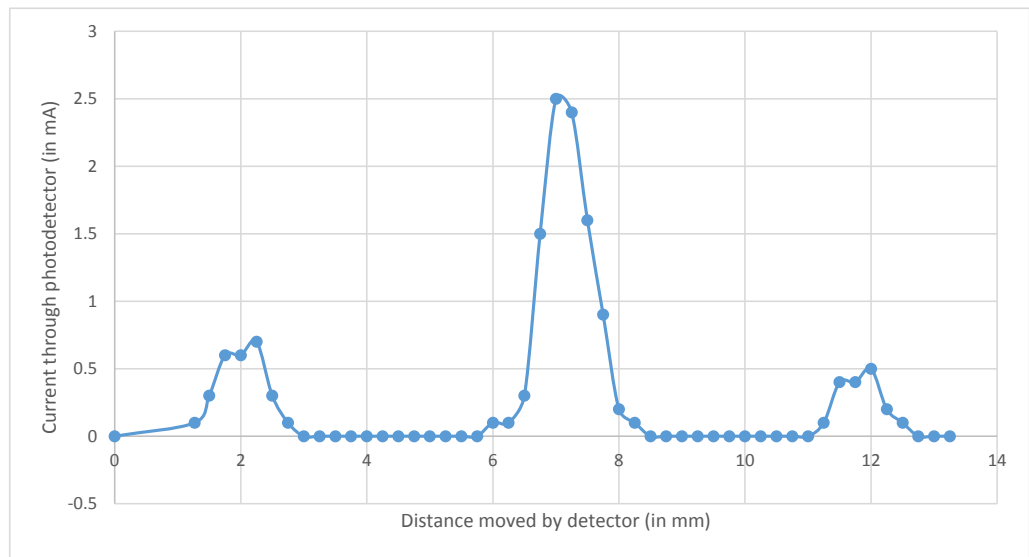


Figure 5: Graph for Acoustic Diffraction

Distance moved by detector (in mm)	Current through photodetector (in mA)
0	0
1.27	0.1
1.5	0.3
1.75	0.6
2	0.6
2.25	0.7
2.5	0.3
2.75	0.1
3	0
3.25	0
3.5	0
3.75	0
4	0
4.25	0
4.5	0
4.75	0
5	0
5.25	0
5.5	0
5.75	0
6	0.1
6.25	0.1
6.5	0.3
6.75	1.5
7	2.5
7.25	2.4
7.5	1.6
7.75	0.9
8	0.2
8.25	0.1
8.5	0
8.75	0
9	0
9.25	0
9.5	0
9.75	0
10	0
10.25	0
10.5	0
10.75	0
11	0
11.25	0.1
11.5	0.4
11.75	0.4
12	0.5
12.25	0.2
12.5	0.1
12.75	0
13	0
13.25	0

Figure 6: Observations for Acoustic Diffraction

Central peak to left peak distance (l1)	4.75 mm
Central peak to right peak distance (l2)	5.00 mm

Distance of detector from grating (D)	$1.303 \pm 0.005$ mm
Wavelength of laser (k)	650 nm
Frequency of RF osc (f)	4.81 MHz
R.I. of water (u)	1.33

Speed of UV sound in water =	$2f(Dk)/ul$
	1312 m/s using l1
	1250 m/s using l2

Error in measuring l1 and l2 can be crudely estimated by measuring the distance of the points adjacent to the peaks and has been found to be around 10%.

Figure 7: Results and Calculations for Acoustic Diffraction

# 3

## NMR

---

September 9 to 30, 2013

### 3.1 $T_1, T_2$

#### 3.1.1 *Minimal Introductory Theory*

##### 3.1.1.1 *Introduction*

A nucleus of an atom has four intrinsic properties: Mass, electric charge, magnetic moment and the so called, ‘spin’. It is important to begin the discussion with the notion of quantization of angular momentum and then reconcile it with the idea of spin. For illustration, consider a rigid diatomic molecule rotating about some axis. This rotating molecule possesses a set of rotational states, in which the total angular momentum  $L_{\text{tot}}$  has one of the following values:

$$L_{\text{tot}} = [J(J+1)]^{\frac{1}{2}}\hbar \quad (13)$$

where  $J$  takes non negative integer values and  $\hbar$  is the reduced Planck’s constant. It is worth mentioning that the quantization is a condition on measurement and not a condition on existence. (Basically, (1) gives a discrete set of eigenvalues for the angular momentum operator.) We might ask if there is any state for which (1) doesn’t hold; but that will be experimentally unobservable and hence irrelevant. Thus,  $J$  completely determines the magnitude of the angular momentum for this system. However, in order to say something about the direction of rotation we need to introduce another quantum number  $M_J$  where  $M_J$  takes up  $2J+1$  integer values from  $-J$  to  $J$ . In the absence of magnetic field, all these  $2J+1$  states are degenerate. However, application of magnetic field breaks this degeneracy. This is called Zeeman effect. The energy separation between the  $M_J$  levels is termed as Zeeman splitting.

Spin is also a kind of angular momentum, however, it is not produced due to the rotation of a particle, but is an intrinsic property of a particle, like mass and charge. Matter is built up in such a way that the spins of the different constituent particles cancel out in any large object. Thus, spin is not visible in the macroscopic world. It is precisely because of this reason that the concept of spin is very abstract and unintuitive; it doesn’t have a classical analogue.

Spin angular momentum  $S_{\text{tot}}$ , is given by the following equation:

$$S_{\text{tot}} = [S(S + 1)]^{\frac{1}{2}}\hbar \quad (14)$$

Here again,  $S$  can only take up a discrete set of values. For some particles,  $S$  is a non negative integer while for some it is a half integer. The former are called bosons, the latter are named fermions. Thus, an elementary particle like an electron can two kinds of angular momentum; one arising from its motion whilst the other being its intrinsic property.  $S$  for an electron is  $\frac{1}{2}$ .

Now consider a system of two particles. The complete system has a total angular momentum quantum number given by either a sum of two individual angular momentum quantum numbers or their difference or any value in between. For example, consider two particles with spin  $\frac{1}{2}$  and  $\frac{1}{2}$ . The spin quantum number of the system can be  $1\frac{1}{2}$ , 2 or  $2\frac{1}{2}$ . Calculating spin for a system of more than two particles is more complicated. For the purpose of this experiment, it suffices to assume that there exists a certain way using which one can describe the spin of the nucleus as a whole. It is reasonable to guess that the total spin of zero corresponds to the state when there is an equal number of nucleons with opposite spin orientations.

### 3.1.1.2 Nuclear spin

Protons and neutrons are made up of quarks. Both are spin  $\frac{1}{2}$  particles. Nuclear spin quantum number is denoted by  $I$ . Now, consider a proton in a nucleus with a mass number  $M > 1$ . The other nucleons can have their spin either parallel or anti-parallel to the first proton. Thus, there is a large number of configurations of spins of nucleons possible for a given nucleus. These nuclear states may have an enormous amount of energy difference among them ( $\sim 10^{11}\text{kJ/mol}$  for  ${}^2\text{H}$ ). There are no simple rules to predict the ground state nuclear spin (the state with the lowest energy), however, a few guidelines are applicable:

1. If the no. of protons and neutrons are both even, the ground state nuclear spin is given by  $I = 0$ .
2. If the no. of protons and neutrons are both odd, the ground state nuclear spin is given by  $I > 0$ .

It is worth highlighting that the splitting between the nuclear ground state and the nuclear excited state is an entirely different phenomenon from the Freeman splitting. The former can be ignored in ordinary spectroscopy owing to the huge energy difference while the latter has magnitude far less than the thermal energies.

### 3.1.1.3 Microscopic magnetism and spin precession

Most of the macroscopic objects are observed to display an induced magnetism in the presence of an external field. The induced magnetic moment takes some time to build up. The equilibrium value of the magnetic moment is proportional to the external magnetic field.

$$\mu_{\text{induced}} = \mu_0^{-1} V \chi B \quad (15)$$

Where  $\mu_0$  is the permeability of the free space,  $V$  is the volume of the object and  $\chi$  is a dimensionless quantity called the magnetic susceptibility expressing how readily the material develops the magnetic moment in the presence of magnetic field.  $\chi$  can be negative as well, in which case the material is said to be diamagnetic. On the microscopic level, there are three fundamental sources of magnetism in an atom:

1. Circulation of electric current due to orbital motion of the electrons.
2. Magnetic moments of the electrons.
3. Magnetic moments of the nuclei.

From Faraday's law (and Lenz' law), it can be guessed that the circulation of electric current contributes a negative value to the susceptibility, whilst the other two have positive contributions. In paramagnetic substances, i.e. the substances with positive  $\chi$ , the latter two contributions dominate over the first. A symmetry rule in quantum mechanics dictates that the spin and magnetic moment operator have the following relation:

$$\hat{\mu} = \gamma \hat{S} \quad (16)$$

For a nucleus,  $\gamma$  is called the gyromagnetic ratio, different for different isotopes. Now, consider a macroscopic bar magnet in an external magnetic field  $B$ . The magnet has a magnetic moment  $\mu$  along its axis. In this scenario, the tendency of the bar magnet is to rotate and orient itself in the parallel (or anti-parallel) to the direction of the applied magnetic field. However, (4) gives rise to a whole new phenomenon in case of quantum particles like nuclei. In this case, there is a precession of angular momentum (and thus, magnetic moment) around the direction of applied magnetic field. Thus spin polarization (direction of spin angular momentum) sweeps a cone around the magnetic field, keeping a constant angle between the spin magnetic moment and the field that depends only on the initial spin polarization. The frequency of this precession is proportional to the external magnetic field.

$$\omega^0 = -\gamma B^0 \quad (17)$$

Where  $\omega^0$  is called the Larmor frequency. The frequency is considered positive according to the right hand thumb rule convention, where thumb points in the direction of  $B$ .

### 3.1.1.4 Spin-lattice relaxation

Spin orientations of nuclei of a typical sample, e.g. H nuclei in water, are uniformly distributed in all the directions, the total magnetic moment being very close to zero. In the presence of a magnetic field, all the nuclei begin executing Larmor precession. However, the atoms which contain these nuclei are undergoing 'collisions' with each other. This thermal motion hence, gives rise to slight fluctuations in the magnetic fields that the nuclei experience. At any given time, the local magnetic field experienced by anyone nuclear spin is slightly different, both in magnitude and direction to its neighbour. These small fluctuating fields due to neighbouring atoms cause a gradual breakdown of constant angle 'cone precession' of the nuclear spins. Over a long period of time, the magnetic moment of each nuclear spin wanders around, moving between different 'precession cones' and eventually sampling the entire range of possible orientations. The time scale of precession motion is a few nanoseconds whilst that of the wandering motion can be as large as a second. The thing to notice is this that since the environment has some temperature, it is slightly more probable that the nuclear spin is driven towards an orientation with higher magnetic energy. This anisotropy of the magnetization distribution in thermal equilibrium means that the entire sample acquires a small net magnetic moment along the field, i.e. a longitudinal magnetic moment. It is found that:

$$\chi_{\text{nuc}} = \frac{\mu_0 \hbar^2 \gamma^2 c}{4k_b T} \quad (18)$$

Where  $c$  is the number of protons per unit volume. Assume that the magnetic moment at equilibrium is denoted by  $M_{\text{eq}}^{\text{nuc}}$ . Magnetic moment of the material after time  $t$  of application of magnetic field to the sample can be approximated by the following relation:

$$M_z(t) = M_{\text{eq}}(1 - e^{-\frac{t}{T_1}}) \quad (19)$$

In the above expression,  $T_1$  is the time constant called the spin-lattice relaxation time constant which depends on the isotope, viscosity and temperature etc.

### 3.1.1.5 Spin-Spin relaxation

The longitudinal nuclear spin magnetization is too weak to be of any experimental importance. The following technique is employed. Suppose that the spin system is allowed to reach a thermal equilibrium,

on microscopic level which corresponds to a large number of nuclear spin magnets precessing around the magnetic field at the same frequency. Let us choose a rectangular coordinate system such that the applied field is in z-direction. There is no net magnetization in the transverse directions. Suppose now an r.f. pulse is applied to the system such that all the spin orientations are rotated by  $\frac{\pi}{2}$  to, say x-directions. Once the pulse is removed, all the nuclei begin to precess around z-axis at an angle of  $\frac{\pi}{2}$ . The net magnetic moment perpendicular to the field applied is called the transverse magnetization. It should be noted that this transverse magnetization will decay with the passage of time because the spin polarizations will cease to precess in synchrony. The factors responsible for making the precession out of sync are lack of homogeneity in the applied magnetic fields, fluctuations in the field due to thermal motion etc. Macroscopic magnetizations at a time t after the pulse has been applied has the form:

$$\begin{aligned} M_y &= -M_{eq}^{nuc} \cos(\omega_0 t) e^{\frac{-t}{T_2}} \\ M_x &= M_{eq}^{nuc} \sin(\omega_0 t) e^{\frac{-t}{T_2}} \end{aligned} \quad (20)$$

It should be noted that there is an exponential decay with a time constant  $T_2$ . This decay constant is termed as the transverse relaxation time constant. It so happens that this rotating magnetic field produces an electric field according to the Faraday's law. If a wire loop is placed at a suitable location near the changing magnetic field, then the electrons of the wire can be brought into motion. Thus a tiny current is generated which can be detected.

### 3.1.1.6 NMR Signal

The oscillating current in the previous expression is called the *NMR signal* or *free-induction decay*. This NMR signal has the information about the Larmor frequency and the time constants.

### 3.1.2 Instrumentation Setup

On a broad level, an NMR spectrometer extracts information about a given sample in three steps.

1. Allowing the magnetic nuclear spins in the samples to reach thermal equilibrium in a large homogeneous magnetic field.
2. Rotating the nuclear spin polarizations by an r.f. pulse.
3. Detecting and amplifying the weak r.f. signals that is emitted as the spins resume their precession motion in the magnetic field.

This poses certain challenges on the machinery. Firstly, the NMR signal is very weak. Secondly the NMR frequencies must be measured

with extremely high accuracies. Thus there are twin challenges of sensitivity and resolution. The spectrometer has following parts:

### 3.1.2.1 *Magnet*

In order to avoid inhomogeneous broadening, the spectrometer uses a magnetic field with extremely high homogeneity (1 part in  $10^9$ ). The NMR spectrometer in the lab employs the use of superconducting magnets. The magnetic field it can produce is of the magnitude 14.7 T. This corresponds to a Larmor frequency of 600 MHz for a TMS Hydrogen. Maintain the superconducting coils (made up of an alloy of Nb and Sn) at a low temperature requires a constant cooling by a bath of liquid helium. The liquid helium bath is itself insulated by another large reservoir of liquid nitrogen. Through the centre of the large cylindrical can of coolant and the superconducting coils there is a large cavity (insulated from the magnets) called bore. The sample is placed on a probe and kept inside the bore so that it experiences the highest magnetic field. The temperature inside the bore can be brought to the room temperature. There are two additional sets of coils called shims. There are two kinds of them: one wound from superconducting material immersed in the liquid helium bath, called superconducting shims and the other supported on a tube that is inserted into the magnet bore, called the room temperature shims. Shims act as a correction for the inhomogeneity of the magnetic field.

### 3.1.2.2 *The Transmitter Section*

This is the part of the spectrometer that produces the r.f. irradiation. In our instrument there were four transmitter sections each dedicated to producing r.f. signals at frequencies close to the Larmor frequencies of different isotopes: C<sup>13</sup>, H, F and D. In general the synthesizer output wave of a transmitter section is given by

$$s_{\text{synth}} \sim \cos(\omega_{\text{ref}}t + \phi(t)) \quad (21)$$

Here  $\phi(t)$  is the r.f. phase while the term  $t$  is the time coordinate. In general, this term  $\phi(t)$  jumps rapidly between different values, the discontinuous phase jumps being controlled by a timing device called the pulse programmer. In general, we need only a short pulse of r.f. and hence it is important to chop out a ‘time-slice’ of the r.f. waveform. This is done by the pulse gate. The duration of an r.f. pulse is termed as the pulse width. Finally, a radio frequency amplifier is used to scale up the gated and shifted waveform so as to produce a large amplitude r.f. pulse.

### 3.1.2.3 *The Duplexer*

The amplified r.f. pulse goes to the probe via duplexer. Another cable emanates from the duplexer which goes to the receiver section. The

role of the device is two fold. It makes sure that the pulse from the transmitter section goes only to the probe and not to the the sensitive receiver section. Secondly, the tiny NMR signal goes only to the receiver and not to the transmitter section. There are multiple ways of doing this but the electronics behind the Duplexer is beyond the scope of this report.

#### 3.1.2.4 *The Probe*

The probe has several functions:

1. Locating the sample in a region of homogeneous magnetic field.
2. Exposing the sample to r.f. waves, detecting the r.f. emissions from the sample.
3. Maintaining the temperature of the sample.
4. Rotating the sample to reduce broadening. (at a frequency of around 10 Hz)
5. Using *cryoprobes* to reduce the temperature of electronic circuits to improvise signal detection.
6. Creating controlled inhomogeneity in magnetic field, often needed in diffusion related and imaging experiments.

#### 3.1.2.5 *The Receiver Section*

The receiver section consists of various sub-parts, the first of which is the signal pre-amplifier, responsible for amplifying the r.f. emission from the sample. Secondly, the quadrature receiver combines the NMR signal, which oscillates at the Larmor frequency  $\omega_{\text{ref}}$ , with the reference signal, oscillating at the frequency  $\omega^0$ , to generate a new signal that oscillates at the relative Larmor frequency  $\Omega = \omega^0 - \omega_{\text{ref}}$ . This is done because for computer analysis, one needs to convert the incoming waveform into a digital signal. However, the present ADC converters can't handle such a high frequency and the latter needs to be brought down, a job accomplished by the quadrature receiver.

### 3.1.3 *Theory*

#### 3.1.3.1 *Prerequisites*

For this section, it is recommended that chapters 10, 11 and 12 are read from Levitt. However, only the following concepts (for spin 1/2 particles) are required for a working knowledge of the experiments.

1. Law of motion of a spin particle under a constant magnetic field and the associated rotation matrices and angular momentum operators

2. Concept of a rotating frame and the transformed Hamiltonian
3. Equation of motion for precession in the rotating frame
4. Effect of an RF pulse on the Hamiltonian \*
5. Understanding of effect of specific pulses like  $(\pi/2)_X$  on the spin particle's state ket
6. Effect of a generalized pulse on the state ket and nutation (a qualitative picture would suffice)
7. Density operator; its need, significance and definition
8. For a spin  $1/2$  system; the physical significance of the terms of the density operator and order of coherence
9. Derivation of the density operator at thermal equilibrium
10. Density operator in the rotating frame
11. Associated to the density operator, the magnetization vector
12. Effect of an RF (strong) pulse on the density operator (using the definition and item 4) \*
13. Effect of specific pulses like  $(\pi/2)_X$  and  $(\pi)_X$  (coherence excitation and population inversion)
14. Free precession without relaxation
15. Phenomenological understanding of transverse and longitudinal relaxation
16. Measurement of  $T_1$  using population inversion and coherence \*
17. Measurement of  $T_2$  using Spin Echo \*

The starred concepts have been discussed in some detail in this report. The notation is identical to that used in Levitt and the meaning of the symbols may be implied from the context.

### 3.1.3.2 *Effect of an RF pulse on the Hamiltonian*

When an RF pulse is applied, the spin particle experiences two magnetic fields, one being the static magnetic field and the other being the oscillating field from the excitation coil. The RF pulse is much weaker than the static magnetic field, but is resonant to the precession frequency of the spin particle. As time goes on, the weak RF field brings about a large change in the spin state.

When an RF pulse of phase  $\phi_p$  along the x-axis of the fixed reference system. The oscillations of the RF pulse oscillating at the spectrometer reference frequency  $\omega_{ref}$ , can be described as the two components rotating in the opposite frequency viz the resonant component

rotating in the same sense as the nuclear spin precession, while the non-resonant component rotating in the opposite.

Neglecting the non-resonant component, the spin hamiltonian during an RF pulse

$$\hat{H} = \omega^0 \hat{I}_z + \hat{H}_{RF}(t) \quad (22)$$

where

$$\hat{H}_{RF}(t) \approx -\frac{1}{2}\gamma B_{RF} \sin \theta_{RF} \cos(\omega_{ref}t + \phi_p) \hat{I}_x + \sin(\omega_{ref}t + \phi_p) \hat{I}_y \quad (23)$$

Apply the sandwich relation to obtain

$$\hat{H}_{RF}(t) \approx -\frac{1}{2}\gamma B_{RF} \sin \theta_{RF} \hat{R}_z(\Phi_p) \hat{I}_x \hat{R}_z(-\Phi_p) \quad (24)$$

where

$$\Phi_p(t) = \omega_{ref}t + \phi_p \quad (25)$$

In rotating frame, the spin Hamiltonian is given by a

$$\hat{H} = \hat{R}_z(-\Phi) \hat{H} \hat{R}_z(\Phi) - \omega_{ref} \hat{I}_z \quad (26)$$

Applying this, we obtain

$$\hat{H} = -\frac{1}{2}\gamma B_{RF} \sin \theta_{RF} \hat{R}_z(-\Phi + \Phi_p) \hat{I}_x \hat{R}_z(\Phi - \Phi_p) + (\omega^0 - \omega_{ref}) \hat{I}_z \quad (27)$$

where

$$\Phi(t) = \omega_{ref}t + \phi_{ref} \quad (28)$$

Finally, upon substitution, we obtain

$$\hat{H} \approx -\frac{1}{2}\gamma B_{RF} \sin \theta_{RF} \hat{R}_z(-\phi_{ref} + \phi_p) \hat{I}_x \hat{R}_z(\phi_{ref} - \phi_p) + \Omega^0 \hat{I}_z \quad (29)$$

where  $\Omega^0$  is the resonance offset. As is visible, there is no time dependence in the expression.

We can also substitute for  $\phi_{ref}$ , for positive spins it equals  $\pi$ ,

$$\hat{H} \approx \omega_{nut} \hat{R}_z(\phi_p) \hat{I}_x \hat{R}_z(-\phi_p) + \Omega^0 \hat{I}_z \quad (30)$$

where the nutation frequency  $\omega_{nut}$  is given by,

$$\omega_{nut} = \left\| \frac{1}{2}\gamma B_{RF} \sin \theta_{RF} \right\| \quad (31)$$

Applying the sandwich relation again,

$$\hat{H} \approx \Omega^0 \hat{I}_z + \omega_{nut} (\hat{I}_x \cos \phi_p + \hat{I}_y \sin \phi_p) \quad (32)$$

### 3.1.3.3 Phenomenological understanding of transverse and longitudinal relaxation

We know the thermodynamically stable populations of a given spin  $\frac{1}{2}$  ensemble. If this population distribution is disturbed, then the system is restored to the equilibrium distribution eventually. This effect is known as longitudinal relaxation, and  $T_1$  quantifies this behaviour.

Similarly, at equilibrium, the coherence is zero. If coherence is introduced, it gradually dies out. This is the transverse relation which is quantified by  $T_2$ .

For  $T_1$ , we have the following phenomenological equations.

$$\rho_{\alpha 3} = (\rho_{\alpha 2} - \rho_{\alpha}^{\text{eq}}) e^{-\tau/T_1} + \rho_{\alpha}^{\text{eq}} \quad (33)$$

$$\rho_{\beta 3} = (\rho_{\beta 2} - \rho_{\beta}^{\text{eq}}) e^{-\tau/T_1} + \rho_{\beta}^{\text{eq}} \quad (34)$$

$$\text{where } \rho_{\alpha}^{\text{eq}} = \frac{1}{2} + \frac{1}{4}\mathbb{B} \quad (35)$$

$$\rho_{\beta}^{\text{eq}} = \frac{1}{2} - \frac{1}{4}\mathbb{B} \quad (36)$$

$T_1$  is typically in the range 100ms - 100s.

For  $T_2$ , we have the following equations that describe the phenomenon.

$$\rho_{-3} = \rho_{-2} e^{(i\omega^0 - \lambda)\tau} \quad (37)$$

$$\rho_{+3} = \rho_{+2} e^{(-i\omega^0 - \lambda)\tau} \quad (38)$$

$$\text{where } \lambda = T_2^{-1} \quad (39)$$

We performed an experiment to find  $\lambda$ , as will be discussed in the next sections.

The precise mechanisms of this process has not been dealt with here and only a phenomenological explanation is provided. However, physically one can think of it as follows. On an average the magnetic field (say along  $\hat{z}$  is constant) is constant and at an instant  $t_0$  the spins are synchronised. However, there always exist some local fluctuations due to the environment of each individual spin which leads to loss of synchronization, and consequently coherence.

### 3.1.3.4 Measurement of $T_1$ using population inversion and coherence

Consider the pulse sequence  $\pi_X \ \tau \ \pi/2_X$  which is repeated for different values of  $\tau$  on a given sample and the data is collected for a fixed  $t$ . The resulting NMR data can be represented using a 2D data matrix =  $S(\tau, t)$ . Before proceeding further, some subtleties have been listed

1. In the actual experiment, the acquisition is repeated to reduce errors
2. Each acquisition is separated by time  $\tau_{\text{wait}}$  to allow the sample to return to thermal equilibrium. ( $\tau_{\text{wait}}$  and  $\tau$  should be much greater than  $T_1$ )

3. Something known as a phase cycle is also performed, but has been ignored here (as was done in Levitt, in this discussion)

Let us now look at what the pulse sequence is really doing and then we'll come to the NMR data and its rudimentary analysis. The action of the pulses on the density operator has been re-written for reference.

- $\pi_x$  generates an inverted population distribution
- $\pi/2_x$  converts the population difference into coherence, including the observable (-1)-quantum coherence.

In terms of the density operator, we can represent the action of the pulse sequence as

$$\hat{\rho}_1 = \hat{\rho}_{\text{eq}} = \frac{1}{2}\hat{I} + \frac{1}{2}\mathbb{B}\hat{I}_z \quad (40)$$

$$\hat{\rho}_2 = R_x(\pi)\hat{\rho}_1 R_x(-\pi) \quad (41)$$

$$= \frac{1}{2}\hat{I} - \frac{1}{2}\mathbb{B}\hat{I}_z \quad (42)$$

$$\hat{\rho}_3 = \frac{1}{2}\hat{I} + \frac{1}{2}\mathbb{B}(1 - 2e^{-\tau/T_1})\hat{I}_z \quad (43)$$

$$\hat{\rho}_4 = R_x(\pi/2)\hat{\rho}_3 R_x(-\pi/2) \quad (44)$$

$$= \frac{1}{2}\hat{I} - \frac{1}{2}\mathbb{B}(1 - 2e^{-\tau/T_1})\hat{I}_y \quad (45)$$

The NMR signal then becomes

$$S(\tau, t) = a(\tau)e^{(i\omega^0 - \lambda)t} \quad (46)$$

$$\text{where } a(\tau) = \frac{1}{2}\mathbb{B}(1 - 2e^{-\tau/T_1}) \quad (47)$$

If we plot  $a(\tau)$  vs  $\tau$ , we expect the graph to start with a negative Y intercept, and monotonically rising and then asymptotically stabilizing at  $y = \frac{1}{2}\mathbb{B}$ .

### 3.1.3.5 Measurement of $T_2$ using Spin Echo

$T_2$  as was described physically earlier, arises from the de synchronization of spins which leads to loss of coherence. We therefore first investigate the concept of peak broadening which is essential to understand the need of spin echo in the first place.

Peak broadening is caused primarily by two factors which are called

1. Homogeneous: This arises due to microscopic magnetic fluctuations (quantified by  $T_2$ ).
2. Inhomogeneous: This is caused by the strong 'macroscopic' magnetic field's inhomogeneity (which is with great pain, attempted to be as homogeneous as possible)

If there were no inhomogeneous broadening, we could easily measure  $T_2$  from the peak broadening. However, there still is a way known as spin echo that can cleverly, selectively measure homogeneous decay, allowing for the measurement of  $T_2$ .

Let us look understand inhomogeneous broadening in a little more depth. Figure 12.6 (from Livett) illustrates how multiple spins, when slightly out of phase, cancel out the effect spin, resulting in a sharper decline, and thus a larger peak width.

In the frequency domain, there are many peaks centred around the peak, which cause the broadening.

We are now ready to discuss the spin echo pulse sequence, the heart of the experiment. The pulse sequence used is  $\pi/2_X \tau/2 \pi_Y \tau/2$  as is given in figure 12.7 of the text. Let's start as usual with the thermal equilibrium state.

$$\rho_1 = \rho^{eq} = \frac{1}{2}\hat{I} + \frac{1}{2}B\hat{I}_z \quad (48)$$

$$\rho_2 = \frac{1}{2}\hat{I} - \frac{1}{2}B\hat{I}_y \quad (49)$$

From this point onwards, no other pulse converts the populations to coherences, thus the  $\hat{I}$  term will be dropped (as it doesn't contribute to the NMR signal).

$$\rho_3 = \frac{1}{2}B(-\hat{I}_y \cos(\omega^0 \frac{1}{2}\tau) + \hat{I}_x \sin(\omega^0 \frac{1}{2}\tau))e^{-\lambda \frac{1}{2}\tau} + \dots \quad (50)$$

$$\rho_4 = \frac{1}{2}B(-\hat{I}_y \cos(\omega^0 \frac{1}{2}\tau) - \hat{I}_x \sin(\omega^0 \frac{1}{2}\tau))e^{-\lambda \frac{1}{2}\tau} + \dots \quad (51)$$

$$\rho_5 = -\frac{1}{2}B\hat{I}_y e^{-\lambda\tau} \quad (52)$$

And from the last step, we know the peak amplitude in the NMR spectrum will be

$$a(\tau) = \frac{1}{2}Be^{-\lambda\tau} \quad (53)$$

Do you see the brilliance of the result? Note that the final density operator is independent of  $\omega^0$ ! Which means that the signal is independent of the (inhomogeneity) applied magnetic field and we have successfully found a way of determining  $\lambda$ .

However, we can gain more insight into this mechanism by geometric considerations; by just staring at figure 12.14 - 12.16.

#### 3.1.4 Practical Implementation

1. Loading the sample
  - a) Ejected the existing item on the air cushion
  - b) Loaded the sample using the stairs

## 2. NMR operation using TopSpin

Following is a summary of the commands executed to obtain the data. The pulse sequences were changed in accordance with the experiment ( $T_1$   $T_2$ ). We were assisted by a PhD student at the NMR lab, with the performance of the experiment.

- a) check no acquisition running
- b) ebc: experiment number, title, check solvent used(we use acetone with D), lock field
- c) rsh: command for shimming which is done artificially using standard samples by making fields homogenous with respect to them and using them as reference.
- d) getprosol: command for retrieving the values of parameters like pulse, duration, delays, aquisition time etc.
- e) lock: command to select solvent, we used AcetoneD6
- f) atma: automatic tuning matching automatically
- g) atmm: automatic tuning matching manually
- h) rga: receiver gain automatic
- i) rgm: reciever gain manual
- j) zg: sets the pulse program t1ir1D, with D1=20s
- k) starts acquiring FID:
- l) efp : command to perform experimental fourier transformation
- m) apk: automatic phase correction
- n) abs: automatic baseline correction, it can be done manually too using the command 'absm'

### 3.1.5 Observations

Upon analysis of the existing experimental data,  $T_1$  was found to be  $7.43 \pm 0.060$ (0.81%) for the first and  $7.92 \pm 0.059$ (0.74%) seconds for the second peak, with the corresponding graphs, [Figure 8](#) and [Figure 9](#) and data, [3.1.5](#). We further found  $T_2$  to be  $78.055 \pm 5.739$ (7.35%) for the first and  $84.762 \pm 5.613$ (6.22%) seconds for the second peak. The corresponding graphs are given in [Figure 10](#) and [Figure 11](#) with the corresponding data in [3.1.5](#).

It is surprising however that we obtained  $T_2 > T_1$  while the theoretic limit is  $2T_1 > T_2$ , which lead us to the implication that the data we analysed was for two different compounds.

The data corresponding to our experiment was lost before it could be recovered from the NMR machine.

D7	Peak 2	Peak 1
0	-0.9949	-1.003

0.2	-0.9846	-1.0488
0.4	-0.9777	-0.9872
0.6	-0.9004	-0.8968
0.8	-0.8631	-0.8452
1	-0.8028	-0.8031
1.2	-0.7569	-0.7365
1.4	-0.7121	-0.6982
1.6	-0.6718	-0.6574
1.8	-0.6211	-0.6055
2	-0.5692	-0.5698
2.2	-0.5427	-0.5172
2.4	-0.5038	-0.4813
2.6	-0.463	-0.4373
2.8	-0.4205	-0.3974
3	-0.391	-0.3584
3.4	-0.3247	-0.2987
0	-0.9794	-0.99
3.8	-0.2489	-0.2104
4	-0.2162	-0.1791
4.2	-0.1854	-0.1397
4.4	-0.1532	-0.1103
4.6	-0.1229	-0.0819
4.8	-0.0887	-0.0467
5	-0.0637	-0.0231
5.5	0.002	0.0494
6	0.0644	0.1234
7	0.2053	0.2559
8	0.2958	0.3479

L4	Peak 2	Peak 1
0.2	0.9921	1
1	0.8541	0.9947
10	0.8674	0.95
20	0.797	0.8583
30	0.6809	0.762
40	0.4647	0.5145
50	0.4851	0.5467
60	0.3192	0.3594
80	0.347	0.2621
70	0.2422	0.2853
90	0.2499	0.241
100	0.2331	0.2219
110	0.2209	0.1975
120	0.1963	0.1781
130	0.2062	0.1715
140	0.1864	0.1683
150	0.1933	0.1582
160	0.1939	0.1547
170	0.1621	0.1563
180	0.1636	0.1541
190	0.156	0.1645
200	0.1521	0.162

210	0.1442	0.1597
220	0.1352	0.1633
230	0.1308	0.1573
270	0.0935	0.1448
250	0.111	0.1502
260	0.1024	0.1465
270	0.0923	0.1398
280	0.0834	0.1329

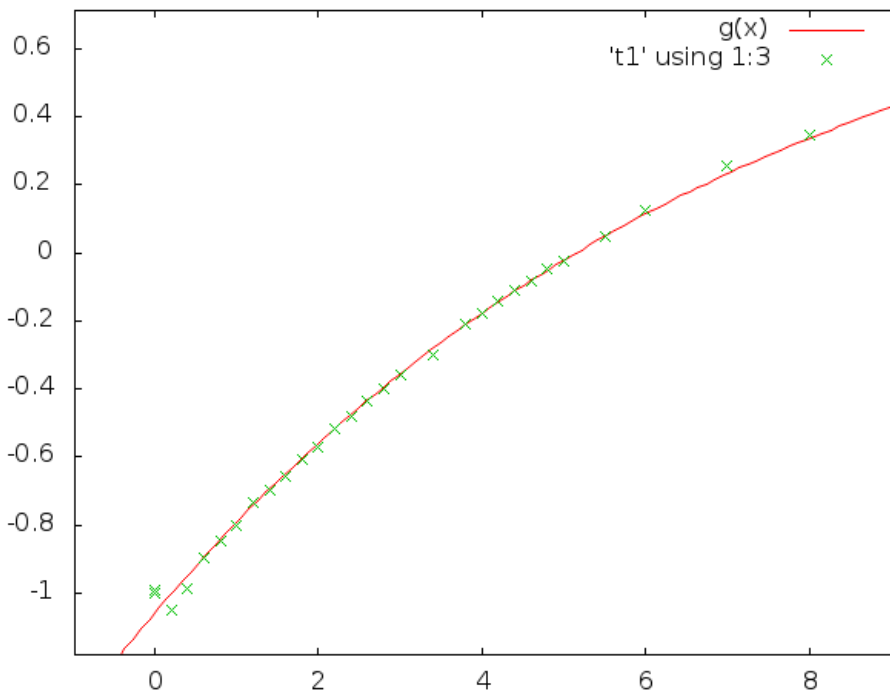


Figure 8: Intensity vs Time (sec), for  $T_1$ , peak 1

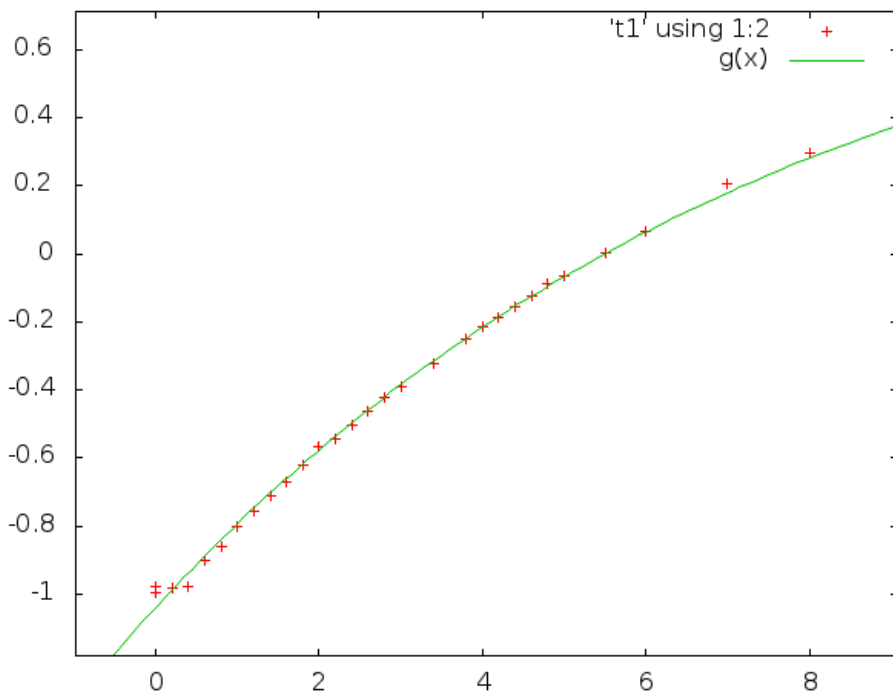
### 3.2 DIFFUSION

There are two important things to understand in this experiment.

- The phenomenon of diffusion and Einstein-Stokes' equation.
- Pulse Field Gradient - Spin Echo (or PFGSE)

#### 3.2.1 Theory

Diffusion is the random translational (or Brownian) motion of molecules or ions across a system driven by its internal thermal energy. Translational diffusion is the basic mechanism by which molecules are distributed in space and plays an important role in any chemical reaction. The systems for which there is an initial concentration gradient, Fick's

Figure 9: Intensity vs Time (sec), for  $T_1$ , peak 2

laws quantitatively explains the relation between the (instantaneous and local) concentration and the flux of the molecules/ions.

Fick's first law postulates that the flux of a material across a given plane is proportional to the concentration gradient across the plane. In other words,

$$J = -D \frac{\partial C(x, t)}{\partial x} \quad (54)$$

Where  $J$  is the flux (Number/meter<sup>2</sup> sec) and  $\frac{\partial C(x, t)}{\partial x}$  is the concentration gradient. The constant of proportionality is called the diffusion constant and has the dimensions of length<sup>2</sup>/time. There is a negative sign to show that molecules/ions are flowing in the direction of lower concentration. The above postulate is sufficient to understand the behaviour of the systems for which the concentration gradient doesn't vary with time. To analyse the variations in concentration due to time, Fick further postulated that the magnitude of change in the local concentration over time is equal to that in local diffusion flux, implying,

$$\frac{\partial C(x, t)}{\partial t} = -\frac{\partial J(x, t)}{\partial x} \quad (55)$$

The above two equations can be combined to give the one dimensional version of the famous diffusion (or heat) equation:

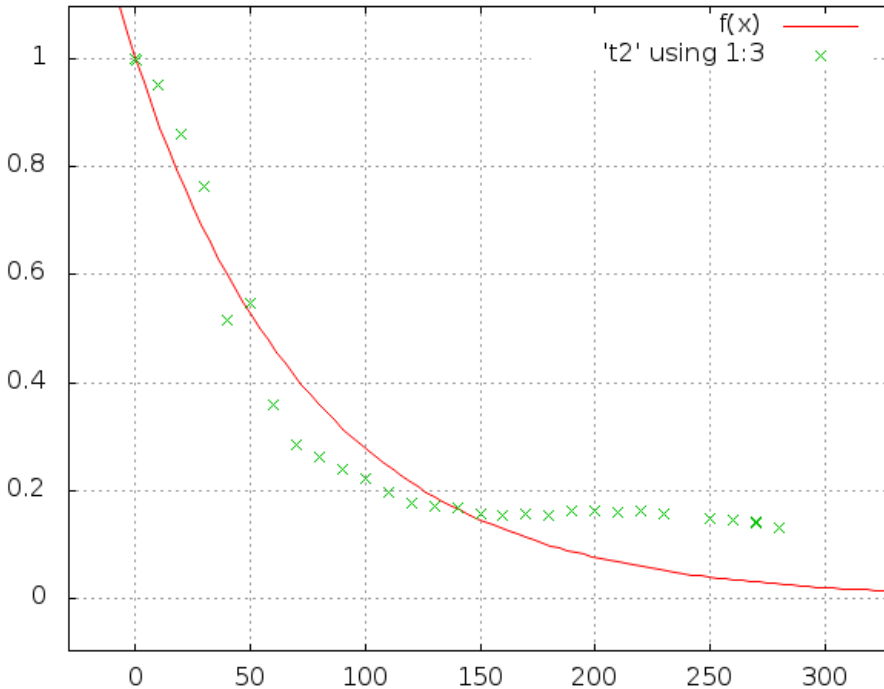


Figure 10: Intensity vs Time, for  $T_2$ , peak 1

$$\frac{\partial C(x, t)}{\partial t} = \frac{\partial^2 C(x, t)}{\partial x^2}$$

It is assumed that the diffusion coefficient is independent of the position. There are three more things to be proven before one can move on to the NMR concepts. Firstly, The mean square value of the displacement of the particles can be evaluated as  $6Dt$ . To prove this, one first needs to find the fundamental solution of the diffusion equation. Let us skip the long procedure of deriving the fundamental solution of the diffusion equation and take it as:

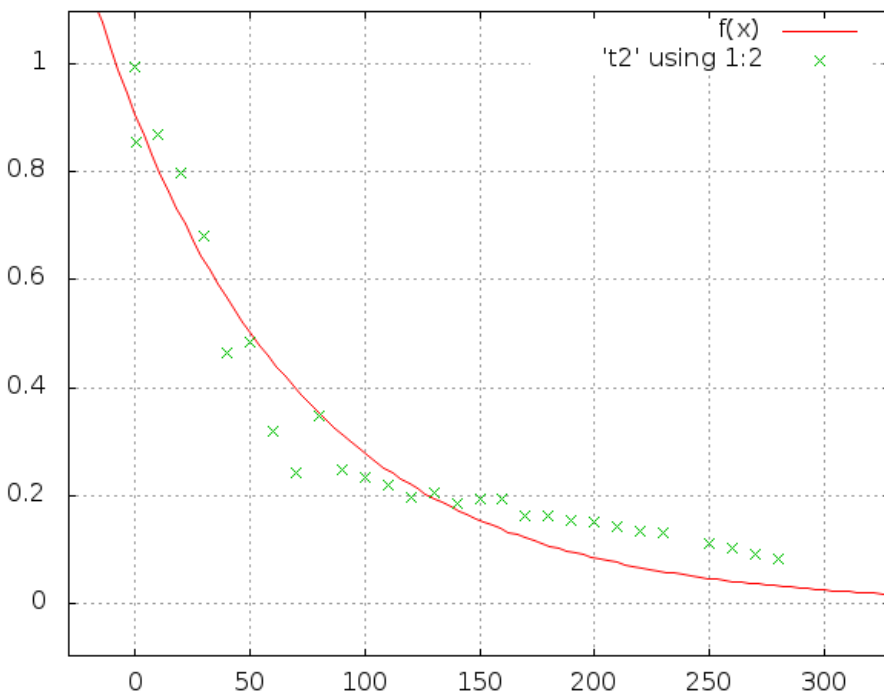
$$P(x, t) = \frac{1}{(\sqrt{4\pi D})^3} e^{-\frac{(x-x_0)^2}{4Dt}} \quad (56)$$

Average of any function  $L(t)$  can now be calculated as:

$$\langle L(t) \rangle \equiv \int_{\mathbb{R}^3} L(x, t) P(x, t) dx \quad (57)$$

Secondly, we need Stoke's law that the force needed to move a small sphere of radius  $R$  through a continuous medium of viscosity  $\eta$  with a velocity  $V$  is given by the following relation:

$$F = 6\pi\eta RV \quad (58)$$

Figure 11: Intensity vs Time, for  $T_2$ , peak 2

Lastly, Einstein-Stoke's equation describes the way that diffusion increases in proportion to temperature, and is inversely proportional to the frictional force experienced by a molecule  $f$ , where  $f = 6\pi\eta R$ . Thus,

$$D = \frac{k_B T}{6\pi\eta R} \quad (59)$$

### 3.2.2 Practical Implementation

In this section we discuss the 'Pulse Field Gradient - Spin Echo' technique.

Let's take a detour and first understand what spin echo sequence means. Imagine that one has a sample where initially the magnetization of the molecules is parallel to the external field.

A  $90^\circ$  pulse is applied along the  $x$  direction so that the net magnetization now lies in the  $xy$  plane, in the  $y$  axis. During the period of time following the removal the RF pulse, each spin experiencing a slight variation in magnetic field begin to fan out slowly or "dephase". The variations in the magnetic field come from both transverse relaxation due to  $T_2$  (spin-spin interaction) and inhomogeneities in the external field. The importance of the spin echo experiment is that the effects of the inhomogeneities are made reversible. At a time  $\tau$  a  $180^\circ$  pulse is applied along the  $y$  direction. The spins are there-

fore rotated by  $180^\circ$  around the  $y$  axis thereby remaining in the  $xy$  plane. As a result of the inverted relative positions, and because each spin continues to precess with its former frequency, all spins will be perfectly re-clustered at time  $2\tau$  forming what is called an echo.<sup>1</sup>

How are this de-phasing and echoing related to diffusion coefficient measurements? Well, imagine now that I have the sample enclosed in a thin tube. If I apply an external magnetic field that varies linearly with height then I should expect a linear variation in the Larmor frequencies. Heterogeneous magnetic field is often supplied by applying two pulses of duration  $\delta$  and constant gradient  $g$  between the  $90^\circ$  and  $180^\circ$  pulse and after the  $180^\circ$  pulse with an interval of time  $\Delta$  between them, in the background of a homogeneous field. If the molecules are now in translational motion then the re-phasing of the spins won't be perfect as the frequency of the spin vector while de-phasing is different from the frequency while re-phasing. This decreases the intensity of the spin echo which can be quantified by the following expression:

$$I(t) = e^{-\frac{2\pi}{T_2}} e^{-D g^2 \gamma^2 \delta^2 (\Delta - \delta/3)} \quad (60)$$

We can vary  $I$  by keeping any 2 quantities out of  $g$ ,  $\delta$ ,  $\Delta$  constant and varying one and do a best fit with equation 7 to obtain  $D$ . In our experiment we varied  $g$  and held all the other parameters constant.

### 3.2.3 Observations and Result

The data obtained has been listed in 3.2.3, where the first column is the percentage of gradient strength, the following columns represent the intensity of two different peaks. Only the first has been used for further analysis in the report. Experimentally,  $\delta = 800\mu\text{s} = 8 \times 10^{-4}\text{s}$ ,  $\Delta = 15\text{ms} = 1.5 \times 10^{-2}\text{s}$ ,  $g = (\text{fraction}) \times 53.5 \times 0.63\text{Gcm}^{-1} = (0.337 \times 10^4\text{Tcm}^{-1})$ ,  $\gamma = 2.675222 \times 10^8\text{s}^{-1}\text{T}^{-1}$  and plugging them into Equation 3.2.2 and taking log on both sides, we get

$$\log I = \text{const} - D \times (7809.87) \times (\text{gradient intensity fraction})^2 \quad (61)$$

$$= \text{const} - D \times (0.780987) \times (\text{GPZ6})^2 \quad (62)$$

Upon curve fitting, we get

$$D \times (0.780987) = -0.000154109 \pm 2.209 \times 10^{-7}(0.1433\%) \quad (63)$$

from which we get  $D = 1.973 \times 10^{-4}(\pm 0.1433\%) \text{cm}^2\text{s}^{-1}$

---

<sup>1</sup> Diffusion measurements by NMR, <http://www.uni-muenster.de/>

GPZ6	Peak 1	Peak 2
95	1	0.9902
85	1.3181	1.3015
75	1.6799	1.6646
65	2.0942	2.0689
55	2.518	2.4861
45	2.9372	2.9003
35	3.325	3.2966
25	3.6431	3.5877

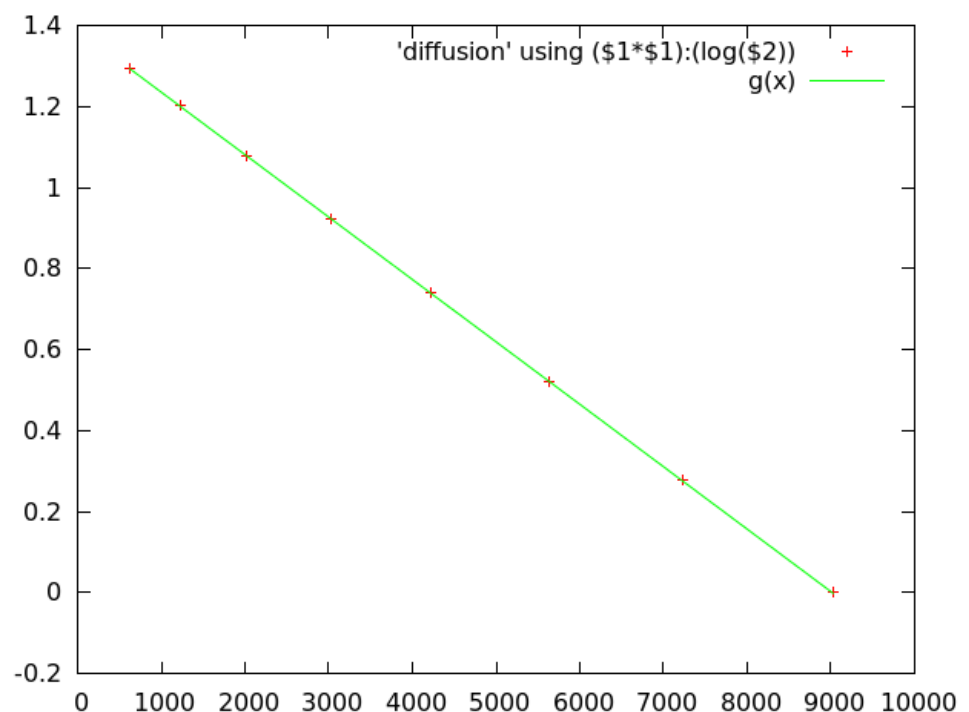


Figure 12: For diffusion,  $\log(\text{Intensity})$  vs Gradient Percentage<sup>2</sup>

# 4

## ZEEMAN EFFECT

---

October 21 to November 4, 2013

### 4.1 INTRODUCTION

We start with a classical description of the Zeeman Splitting and Polarization, beginning with justifying how we can model the Atom as a harmonic oscillator. Next, we'll discuss the Fabry Parot device and its basics. We'll then go on to discuss how it operates to produce fringes in various setups. We then briefly mention the constant deviation spectrometer and finally, discuss the setup of the two related experiments.

### 4.2 CLASSICAL DESCRIPTION OF ZEEMAN SPLITTING

#### 4.2.1 *Modeling the Atom as a harmonic oscillator*

Consider a simple atomic system with a heavy nucleus and a light electron. In the rest frame of the electron, at equilibrium we can write

$$m_e a_0 = 0 = \frac{m_e v^2}{r_0} - \frac{kq^2}{r_0^2}$$

where radially inwards direction has been taken as negative and  $r_0$  is the radius of the orbit. However, if we displace the the electron from its equilibrium trajectory, and assume the velocity remains unchanged, we can write

$$m_e a = \frac{m_e v^2}{r_0 + r} - \frac{kq^2}{(r_0 + r)^2}$$

We can now taylor expand both the force term and the pseudo force to obtain

$$m_e a = m_e v^2 \left( \frac{1}{r_0} - \frac{r}{r_0^2} + \frac{r^2}{r_0^3} + \dots \right) - kq^2 \left( \frac{1}{r_0^2} - \frac{2r}{r_0^3} + \frac{3r^2}{r_0^4} + \dots \right)$$

where  $r$  is the perturbation from the equilibrium point (radially outward corresponds to  $r > 0$ ). Keeping only leading order terms and applying the equilibrium relation, we get

$$m_e a = \left( -\frac{mv^2}{r_0} + \frac{2kq^2}{r_0^3} \right) r = -m\omega_0^2 r$$

where we have

$$\omega_0^2 \equiv \left( \frac{v^2}{r_0} - \frac{2kq^2}{mr_0^3} \right)$$

Although we haven't shown  $\omega_0$  to be real, we assume it to be so. This explains why we can model to first order, a simple (hydrogen) atom, as a harmonic oscillator.

#### 4.2.2 Zeeman Splitting and Polarization

It is established now that an atom in a magnetic field can be modelled as a simple harmonic oscillator. Let  $\omega_0$  be the frequency of motion in the absence of magnetic field; the electron has the same resonant frequency in motion along  $x$ ,  $y$  and  $z$  directions. In the presence of magnetic field  $B$ , the equation of motion, in the rest frame of electron is given as

$$m_o \frac{dv}{dt} = -m_o \omega_0^2 r - ev \times B$$

where the  $r$  is the position vector and  $v = \dot{r}$  is the velocity vector. If the direction of the field is along the  $z$  axis,  $B = B\hat{e}_z$

$$\ddot{r} + 2\Omega_L \dot{r} \times \hat{e}_z + \omega_0^2 r = 0$$

where  $\Omega_L$  is the Larmor frequency defined as

$$\Omega_L = \frac{eB}{2m_o}$$

Applying the matrix method to solve the above equation, we look for a solution in the form of a vector oscillating at  $\omega$  such as

$$r = \text{Re} \left\{ \begin{pmatrix} x \\ y \\ z \end{pmatrix} \exp(-i\omega t) \right\}$$

and obtain the following matrix

$$\begin{pmatrix} \omega_0^2 & -2i\omega\Omega_L & 0 \\ 2i\omega\Omega_L & \omega_0^2 & 0 \\ 0 & 0 & \omega_0^2 \end{pmatrix} \begin{pmatrix} x \\ y \\ z \end{pmatrix} = \omega^2 \begin{pmatrix} x \\ y \\ z \end{pmatrix}$$

we then find the eigen values by building the following determinant

$$\begin{vmatrix} \omega_0^2 - \omega^2 & -2i\omega\Omega_L & 0 \\ 2i\omega\Omega_L & \omega_0^2 - \omega^2 & 0 \\ 0 & 0 & \omega_0^2 - \omega^2 \end{vmatrix} = 0$$

which then gives

$$\{\omega^4 - (2\omega_0^2 + 4\Omega_L^2)\omega^2 + \omega_0^4\}(\omega^2 - \omega_0^2) = 0$$

By inspection,  $\omega = \omega_0$  is one solution. For  $\Omega_L \ll \omega_0$ , the approximate frequencies are  $\omega \approx \omega_0 \pm \Omega_L$ . The eigen vectors corresponding to these

$$\mathbf{r} = \begin{pmatrix} \cos(\omega_0 - \Omega_L)t \\ -\sin(\omega_0 - \Omega_L)t \\ 0 \end{pmatrix}, \begin{pmatrix} 0 \\ 0 \\ \cos(\omega_0 t) \end{pmatrix}, \begin{pmatrix} \cos(\omega_0 + \Omega_L)t \\ \sin(\omega_0 + \Omega_L)t \\ 0 \end{pmatrix}$$

the motion along  $z$  axis is not affected by the magnetic field and the angular frequency remains  $\omega_0$ . The off diagonal terms  $\pm 2i\omega\Omega_L$  of the matrix depict the coupling of the motions in the  $x$  and  $y$  directions resulting in circular motion confined to the  $xy$  plane, with frequencies shifted from the Larmor frequency  $\omega_0$ . Evidently the applied external field separates the initially equal frequencies.

The direction of radiation is given by the  $\mathbf{a} \times \mathbf{r}$ , where the  $\mathbf{a}$  is the acceleration and  $\mathbf{r}$  is the position vector of the electron.

The electron oscillating parallel to  $\mathbf{B}$  radiates with angular frequency  $\omega_0$ , in the  $y$  direction when seen in the  $xy$  plane, and no radiation is observed in the direction of the magnetic field.

The circular motion of the electron produces radiation with angular frequencies  $\omega_0 + \Omega_L$  and  $\omega_0 - \Omega_L$ . Looking edge-on, this circular motion is seen as a linear sinusoidal motion. Seeing along the  $y$  axis, the linear motion is along the  $x$  axis, and the radiation is polarised perpendicular to the magnetic field. Looking along the  $z$  direction, the motion is circular and the radiation is circularly polarised, associated with the respective frequencies.

#### 4.2.3 Limitations

Other than the inconsistencies of the assumptions, the fact that we need a discharge tube for observing the effect is not explained. For the purposes of this experiment, postponing the precise quantum mechanical description for later, I would just state that radiation we observe is when the electron jumps down an ‘orbit’. This essentially means that two given ‘orbit’ is split and due to selection rules, we see only three wavelengths of radiation, shifted up, shifted down and the original (before application of the magnetic field).

Another peculiar result seems to be that the eigenvector passes through the centre of the atom! This is a sort of projection, or so we were told. We weren't able to identify the source of this error.

### 4.3 FABRY PAROT

This is a very elegant device. This harnesses a principle very similar to that of the interferometer. Instead of explaining in words, let's derive it straight away. Consider a ray incident on the etalon at an angle  $\theta$  with respect to the outward normal of the first surface. The corresponding virtual ray (with respect to the second surface) can be constructed a distance  $2d$  behind the real ray. Considering that the distance between the screen and the etalon,  $D \gg d$ , to see interference we simply need to consider the path difference between these two rays, along a plane whose normal coincides with the ray. As shown in the diagram, it follows this distance is

$$\Delta\lambda = 2d \cos \theta$$

This now has very interesting repercussion. If you have a monochromatic point source incident, depending on the angle of a ray with the normal of the etalon surface, you would get a path difference. This results in the formation of circular fringes with constructive interference happening on specific radii (explicit calculations have been done in the next experiment). If there was another monochromatic source at the same location, you would again get a circular pattern corresponding to the new wavelength. Keep this in mind. We'll use this property often.

#### 4.3.1 *The effect of sources and lenses*

It is important to understand in some detail what happens under the permutation of the following conditions

1. Monochromatic Source
  - a) Point
  - b) Extended
2. Lens
  - a) Before (the source is on the focal plane)
  - b) After (if you remove the lens and look directly, it is equivalent, the eye has a lens)
3. [not discussed] Eye after lens

So there will be  $2^3 = 8$  possibilities. Let's do them all. Consider a Monochromatic:

1. Point Source, without any lens

This was discussed earlier in this section. The result is *circular fringes*.

2. Extended Source, without any lens

The point source and the etalon can be effectively treated as two point sources,  $2d$  distance apart ( $d$  is as usual, the distance between the mirrors of the etalon). Using superposition, we can claim the pattern should be a superposition of multiple circular fringes, corresponding to every point of the source. Effectively, *no pattern* should be visible.

3. Point Source, with a lens before, but none after

The result is that all the light rays incident on the etalon would be parallel. Thus a uniform intensity pattern should be obtained, and changing the angle of the etalon with respect to the principle axis of the lens ( $\theta$ ) should yield *different uniform intensities*.

4. Extended Source, with a lens before, but none after

In this case, each point on the extended source is mapped to a parallel light beam of a fixed angle  $\theta$  with respect to the principle axis, as a function of its (the point's) distance from the principle axis. The etalon will simply add a phase difference of  $2d \cos \theta$  to a beam of a given orientation. Since there's no lens after, all these will fall on a screen and result in a *uniform intensity, independent of the orientation of the etalon*.

5. Point Source, with a lens before and a lens after

The image obtained will be that of a *single point*, except it would be either bright or dark, *depending on the orientation* of the etalon ( $\theta$ ).

6. Extended Source, with a lens before and a lens after

The analysis from the previous part follows. The other lens focuses parallel beams on different points on the focal plane, essentially mapping  $\theta$  to position. Since the phase difference depended on angle  $\theta$ , thus different points on the screen would be bright or dark, depending on its value. Symmetry considerations immediately tell us that the pattern will be *circular fringes* (may be cropped though, depending on the shape of the extended source).

[‘Prism’ zeeman like]

7. Point Source, without a lens before, but with a lens after

This is perhaps the most non-trivial case. Again, we effectively have two point sources, but they are followed by a lens (both points are farther away from  $2F$ ). Using the limiting size case, one can find the resultant position of the image for both points. Now the problem has been significantly been simplified. Given

some position of the screen (taken to be the focal plane of the lens here), for any given point on the screen, we construct two lines (representing the rays); the first joining the first point's image and the screen point and the second joining the second point's image and the screen point. Extending this line, we can find the point of intersection with the lens. Now we connect the intersection of the first line with the lens, with a line to the first source point. Similarly for the second point we repeat the procedure. Using this, one can calculate the path difference between the two rays that superpose on the screen. Without quantifying, from the symmetry, it is clear that a *circular pattern* will again be obtained in this case.

[‘TV’ Zeeman like if you consider the source to be a point source]

8. Extended Source, without a lens before, but with a lens after  
Here again, a *circular pattern* is obtained. This can be easily understood again by considering two extended sources. Now we consider only parallel beams coming from the corresponding points of the two sources, for other beams (non parallel) will either not be focussed or (different points, but parallel) not coherent. As earlier, the etalon will add a phase difference depending on the angle  $\theta$ , and the lens will converge at a location, depending again on  $\theta$ . Thus, we get the aforesaid pattern.

[Michelson, ‘TV’ Zeeman like]

Note however that if the object is placed between  $F$  and  $2F$  (where  $F$  is the focal point of the lens) then one can simply substitute the source to be placed at the point where the image will be formed, had a screen been placed there; then the setup can be matched to the possibilities given above and proceed accordingly. Further, in case of a point source along the principle axis, we can find the image position by first finding the same for an extended source and then take its size limit to zero.

#### 4.4 CONSTANT DEVIATION SPECTROMETER

In a usual spectrometer, the wavelength resolved beam is not parallel. This uses a prism as shown in the diagram in the last section. This prism produces a parallel resolved beam. The details haven't been worked out for this part of the apparatus wasn't used for calculations.

#### 4.5 THE SETUP

##### 4.5.1 *The ‘TV’ Zeeman (polarization)*

The setup consists of an electromagnet ([Figure 17](#)), built with two coils and a mercury cadmium lamp placed in the centre. The light

can be seen through the axis of the coils as well as through a direction perpendicular to it. This assembly is mounted on a rotatable, well, mount. Adjacent to the mount, there's an optical bench. The bench has a lens that results (eventually) in a diverging beam. This is followed by the all glorious etalon. Then we have two polarisers which are then viewed through a magnifier on the screen using a camera.

Let us now understand what is happening. We start without polarisers. This is the same as an extended source without a lens before (the object is not at the focus of the lens) and a lens after. However, the source is not monochromatic, instead it has three wavelengths. Their circular patterns superimpose. Further, as explained in the earlier sections, the different frequencies are polarized differently. The polarized can be inserted to block lights of specific frequencies and the fringe pattern corresponding to that wavelength disappears; resulting in a higher contrast pattern.

#### 4.5.2 The 'Prism' Zeeman (splitting)

The setup consists of collimator (Figure 15), a special constant deviation prism, and a telescope. The collimator has an adjustable slit width. Incident to this can either be a sodium or mercury lamp, or a Neon discharge tube, placed between two coils of an electromagnet.

Let us look at what is happening. The setup starts with converting the incident light into the shape of the slit. Then this light is passed through the collimator. The collimator is focussed such that the point source is in its focal plane (this is leading to a type 6 setup). This is then incident on the prism, which does two things. It guides the light into the telescope; and it spatially displaces different wavelengths. So effectively, the different frequencies have become spatially displaced sources. Since the shape of the extended source is a slit, introduction of an etalon results in the creation of slits in the line (instead of the circular fringes). Upon application of the magnetic field, a single frequency splits into three, and so does the corresponding pattern. What remains to show is that this splitting distance is directly proportional to the applied magnetic field, and that was the experiment we performed.

The observations are given in 4.5.2 where the column names are self explanatory, the calibration of the current and magnetic field are given in 4.5.2, while the corresponding graphs are Figure 13 and Figure 14.

Centre	Top	Bottom	Current	Difference
9	44	24	3.18	30
9	47	20	2.5	23
8	46	21	2.49	25
9	50	19	1.96	19

8	51	15	1.46	14
9	51	16	1.46	15
	54	12	1.08	8
	53	11	1.08	8

## Amperes 10 Gauss

0	18
0.25	111
0.45	185
0.7	282
0.92	368
1.1	441
1.35	546
1.51	603
1.74	695
1.95	776
2.29	900
2.54	988
2.73	1053
2.98	1127
3.19	1182
3.06	1158
2.84	1104
2.62	1037
2.34	945
2.18	884
1.81	741
1.5	622
1.28	536
1.08	453
0.83	353
0.53	234
0.29	136
0.11	66
0	20

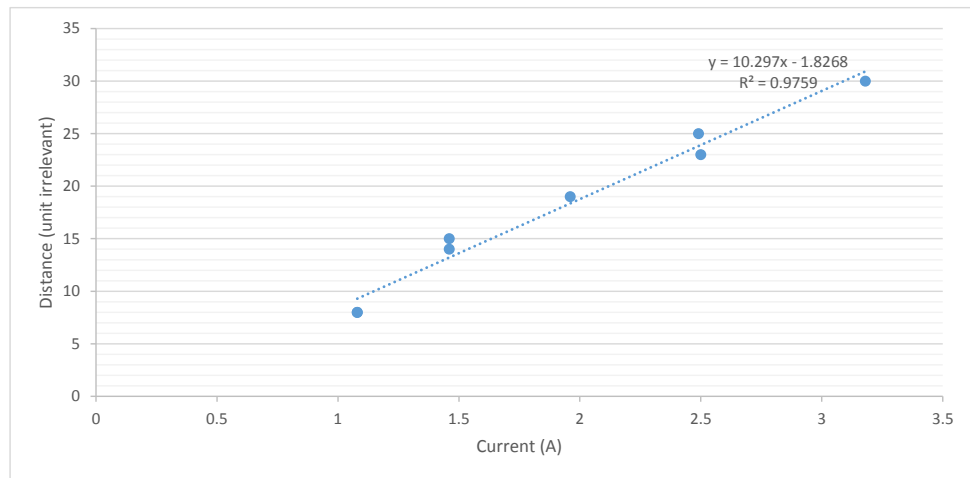


Figure 13: Split Distance vs Current

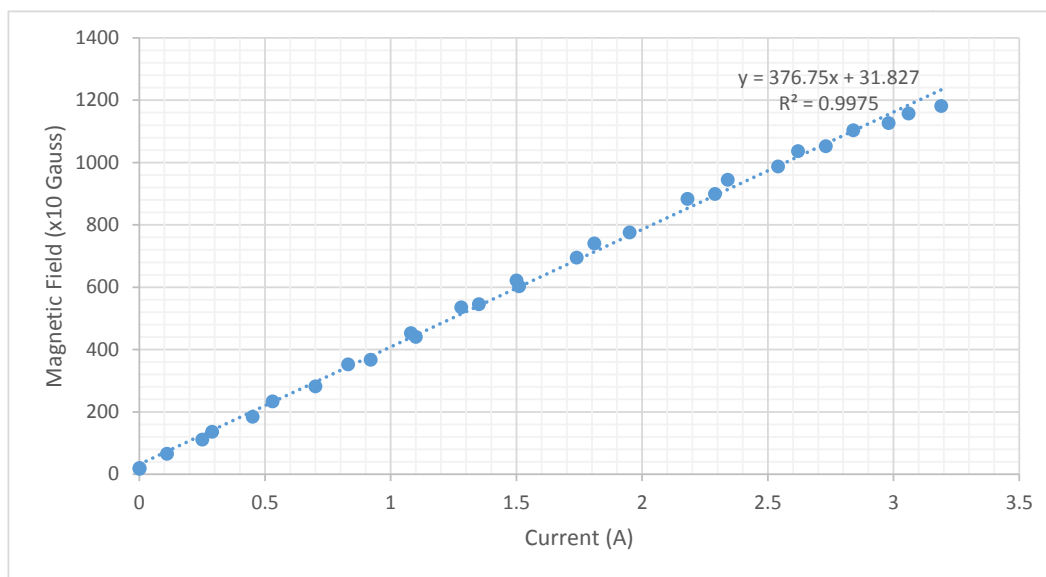


Figure 14: Calibration of Magnetic Field and Current

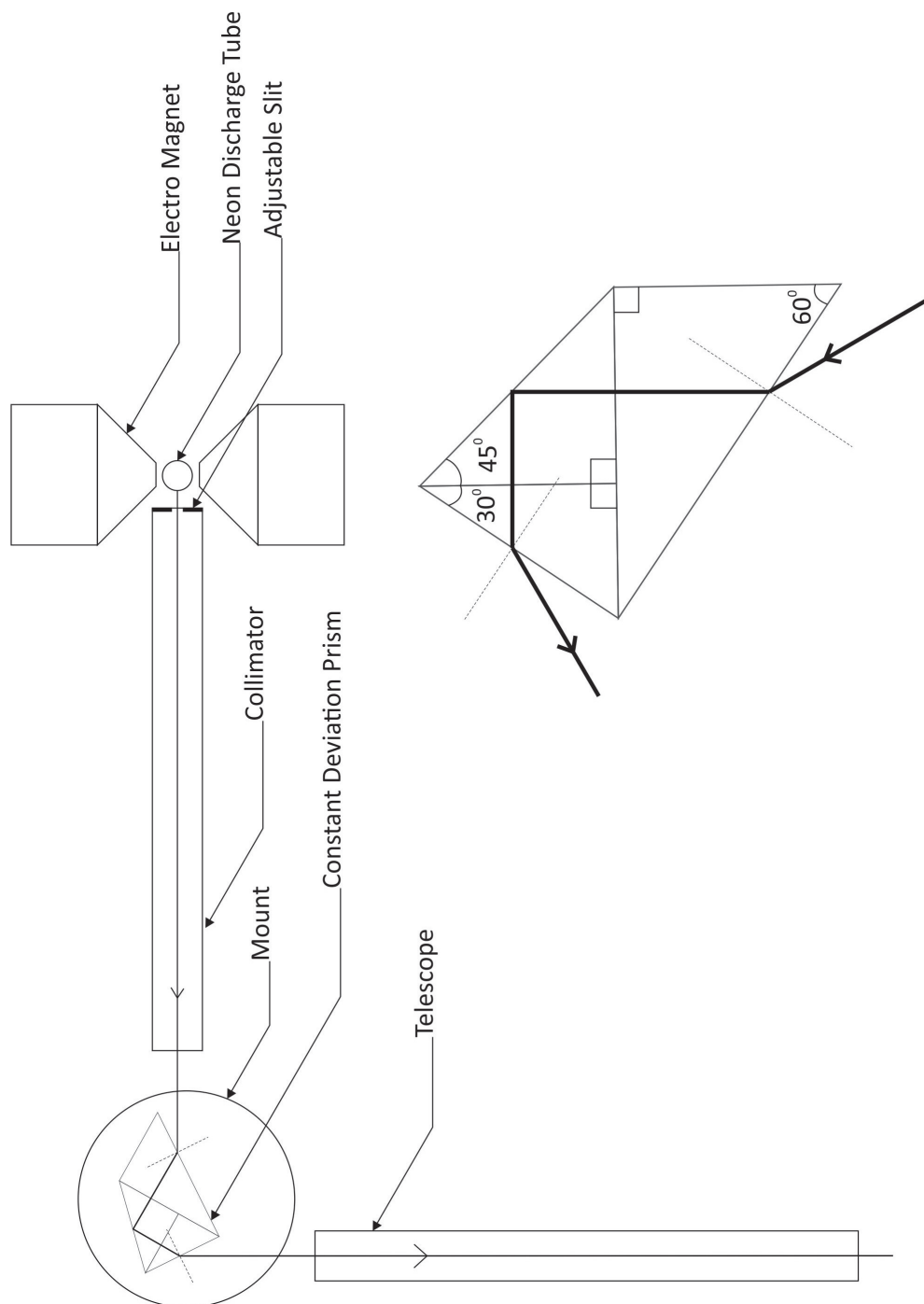


Figure 15: 'Prism' Zeeman Setup

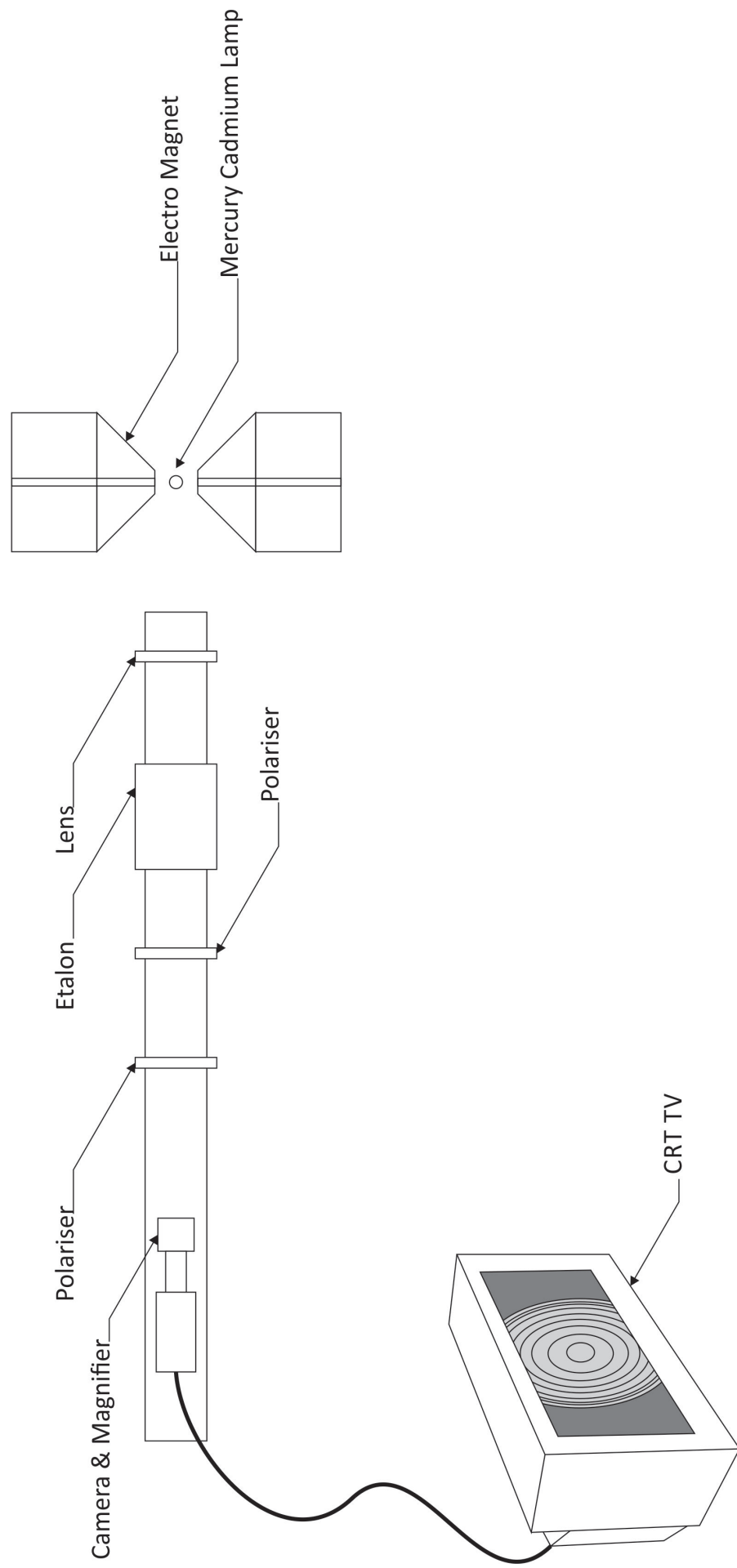


Figure 16: 'TV' Zeeman Setup

# 5

## FABRY PEROT

---

November 4 to 19, 2013

### 5.1 CALIBRATING THE FABRY PEROT

Let us start with the assuming that you have a bright fringe at the centre. Let the distance initially between the two mirrors of the etalon be  $d_1$ . So in this situation we have

$$2d_1 = n\lambda$$

Where  $n$  is some arbitrary number, and  $\lambda$  is wavelength of light. Now suppose you move one of the mirrors such that the new distance is  $d_2 = d_1 + \Delta d'$ , where  $\Delta d'$  is what you measure using the screw guage. Also, let us assume that the centre is bright again, and a total of  $m$  fringes collapsed to the centre in the process of changing the distance. Then, ideally we must have

$$2\Delta d' = m\lambda$$

We know all the quantities in the equation. However, in practice, there'll be some error, which can be removed by calibration. Thus we define the expected distance by

$$\Delta d \equiv m\lambda/2$$

And we define our calibration constant

$$C = \frac{\Delta d}{\Delta d'}$$

### 5.2 DETERMINING THE SPACE BETWEEN THE MIRRORS OF THE ETALON

The analysis for this part rests on the assumption that effect displayed in the following figure can be neglected. We'll show later by simple calculations the range of the radius for which this can be neglected.

We start simple. From trigonometric arguments, we have the following relation between the angle  $\theta_m$  of a ray from the source to

the screen<sup>1</sup>, corresponding to a bright fringe, where  $m$  is a number (which will be defined soon), and  $r_m$ , the radius of the ring on the screen.

$$\frac{r_m}{D} = \tan \theta_m$$

For small angles, we have

$$\tan \theta_m = \theta_m = \frac{r_m}{D}$$

Now we look at the  $n$ th large bright ring from the aforesaid ring. For this also, we correspondingly have

$$\tan \theta_{m+n} = \theta_{m+n} = \frac{r_{m+n}}{D}$$

We now give meaning to number  $m$ . For the first ring, the condition for being bright is given by

$$2d \cos \theta_m = m\lambda$$

where  $\lambda$  is the wavelength of the incident laser light. Then it follows that

$$2d \cos \theta_{m+n} = (m-n)\lambda$$

where the minus sign is owing to the fact that we've assumed the larger ring to correspond to  $\theta_{m+n}$ , which implies  $\theta_{m+n} > \theta_m$ .

We eliminate  $m$  from these equations to obtain

$$2d(\cos \theta_{m+n} - \cos \theta_m) = -n\lambda$$

If we use small angle approximation for  $\cos \theta = 1 - \theta^2/2$ , we get

$$d(\theta_{m+n}^2 - \theta_m^2) = n\lambda$$

which in terms of observables, is

$$\frac{r_{m+n}^2 - r_m^2}{D^2} = \frac{n\lambda}{d}$$

So finally we have

$$d = \frac{n\lambda D^2}{r_{m+n}^2 - r_m^2}$$

<sup>1</sup> with respect to the line joining the centre of the pattern and the source

### 5.2.1 Small Angle Approximation

We have assumed that the analysis given above works, so long as the distance  $2d \tan \theta < 1\text{mm}$ , the least count of the radius measurement apparatus. We then find the range of  $\theta$  for which this is valid and thereby determine the radius of fringes we can use, without the theory failing. The  $d \approx 2\text{cm}$  in our setup, so we get  $\theta < 0.025$ , and using  $\theta \approx \tan \theta = d/D$ , with  $D = 70\text{cm}$ , thus the radius must have the following constraints

$$r < 1.75\text{cm}$$

for confident results.

## 5.3 THE SETUP

The setup has very curious similarities with the Michelson interferometer. First note that in the Michelson interferometer, there are three cases to be considered

1. Point source (the black paper with hole doesn't function as a very good point source)
2. Non coherent extended source (the diffuser case)

In the first case, we would obtain a pattern on a screen, but won't be able to see it. In the second case we won't see it on a screen. However we (experimentally known) can see it directly.

One could verify these results in the Fabry Perot setup as well. With a point source (the diode laser, with or without an additional lens), when viewed through the fabry perot, doesn't yield a pattern, although you get it on a screen. Conversely, if you converted the point source into an extended source, the pattern on the screen disappears, however you can now observe it directly through the etalon. In complete agreement with the predictions.

## 5.4 OBSERVATIONS AND RESULTS

The observations corresponding to distance estimation have been listed in [5.4](#), where the distances have been measured in mm. The distance between the mirrors was found ([5.4](#)) to be  $2.67 \pm 5\%$  mm.

The observations for calibration have been listed in [5.4](#) and the calculations ([5.4](#)) show the calibration constant was  $2.95 \times 10^{-3} \pm 3.2\%$ .

No	Out	In	Rad	Rad^2	N=5	N=1
12	6.0	104.6	49.30	2430.49	850.43	226.19
11	8.4	102.3	46.95	2204.30	835.30	201.74
10	10.5	100.0	44.75	2002.56	808.86	234.36

9	13.3	97.4	42.05	1768.20	822.64	188.14
8	15.5	95.0	39.75	1580.06	859.14	211.06
7	18.0	92.0	37.00	1369.00	849.16	175.30
6	20.6	89.7	34.55	1193.70	882.18	248.14
5	24.0	85.5	30.75	945.56	824.56	224.64
4	27.9	81.6	26.85	720.92		201.08
3	32.0	77.6	22.80	519.84		208.32
2	37.0	72.3	17.65	311.52		190.52
1	43.0	65.0	11.00	121.00		

	Average	StdDev	Error (%)
N=5	841.53	23.5	2.79
N=1	209.95	21.8	10.37
Dist	2.67	5	mm

MSR (mm)	CSR	Displacement (mm)
1	1	1.01
1	8	1.08
1	12	1.12
1	14	1.14
1	11	1.11
1	9	1.09
1	10	1.10
1	8	1.08
1	7	1.07
1	6	1.06
1	12	1.12
1	13	1.13
1	15	1.15
1	12	1.12
1	14	1.14
1	10	1.10
	1.10	<Average
	0.03	<Standard Deviation
	3.2	<Percent Error

Wavelength of diode laser	650 nm
Displacement for 10 readings	0.00325 mm
Calibration Constant	0.002951192 (3.2% error)

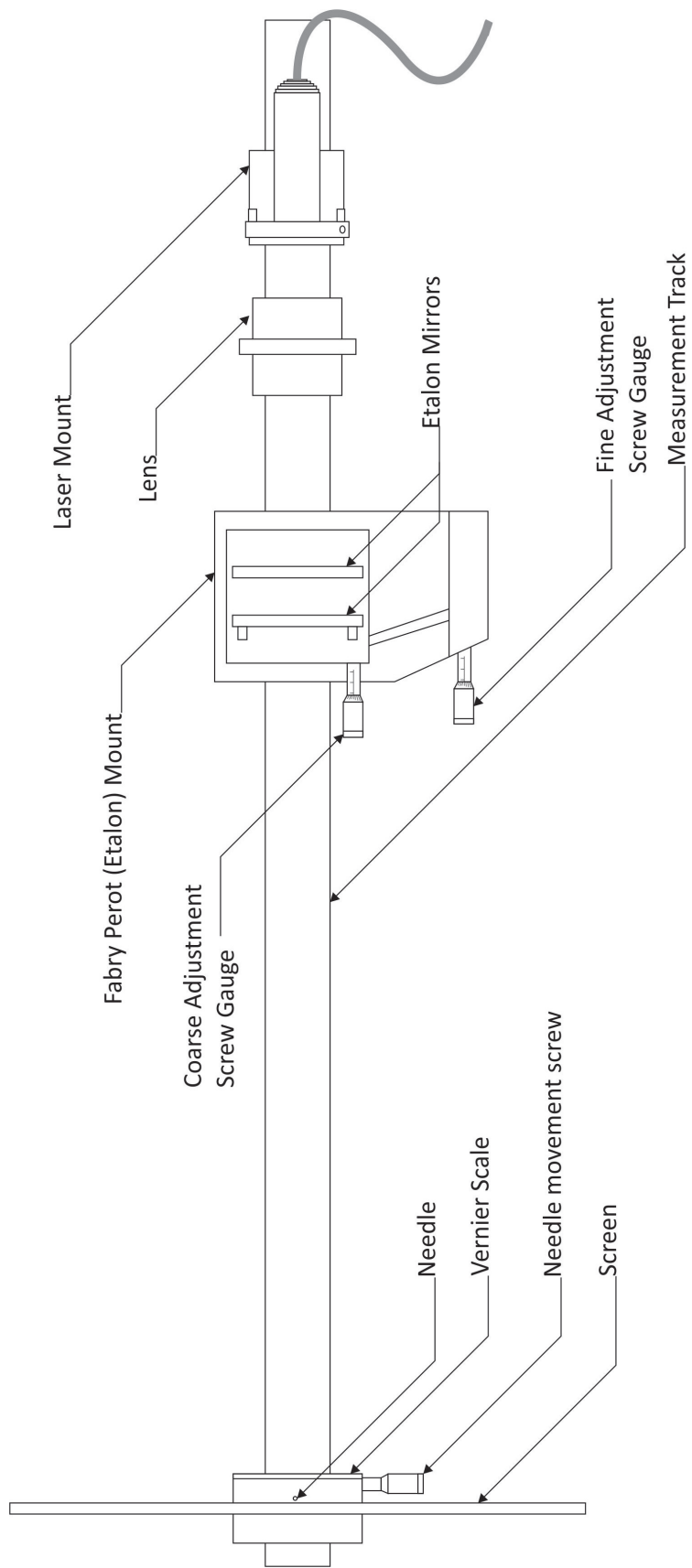


Figure 17: The Fabry Perot Setup



## COLOPHON

This document was typeset using the typographical look-and-feel `classicthesis` developed by André Miede, for L<sup>A</sup>T<sub>E</sub>X.  
The style was inspired by Robert Bringhurst's seminal book on typography "*The Elements of Typographic Style*".

The latest version of this document is available online at:

[https://github.com/toAtulArora/IISER\\_repo](https://github.com/toAtulArora/IISER_repo)